Chapter 4 Thermal Infrared Radiation Transfer in the Atmosphere

4.1 The Thermal Infrared Spectrum and the Greenhouse Effect

Based on data gathered from satellite radiation budget experiments, the earth–atmosphere system reflects about 30% of the incoming solar radiation at the top of the atmosphere and absorbs the remaining part (see Section 8.2 for further discussion). Absorption and scattering of solar radiation take place in the atmosphere, processes that were discussed in Chapter 3. A large portion of the incoming solar radiation is absorbed by the earth's surface, consisting of approximately 70% ocean and 30% land. Over a climatological period of time, say, over a year or longer, the global equilibrium temperature of the earth–atmosphere system remains relatively constant. Consequently, radiant energy emitted from the sun that is absorbed in the earth–atmosphere system must be re-emitted to space so that an equilibrium energy state can be maintained. Just as the sun emits electromagnetic radiation covering all frequencies, so do the earth and the atmosphere, and this emitted radiation is referred to as *thermal infrared radiation*.

On the basis of the conservation of absorbed solar and emitted thermal infrared energies, and denoting the global albedo of the earth–atmosphere system by $\bar{r}$, the Stefan-Boltzmann law for emission gives us the following balanced equation:

$$S \cdot \pi a_e^2 (1 - \bar{r}) = \sigma T_e^4 \cdot 4\pi a_e^2, \tag{4.1.1a}$$

where a_e is the earth's radius, S is the solar constant, representing the energy available at the top of the atmosphere, and T_e denotes the equilibrium temperature of the earth–atmosphere system. The factor of 4 accounts for the difference between the absorption and emission areas. Thus, we obtain

$$T_e = [S(1 - \bar{r})/4\sigma]^{1/4}. \tag{4.1.1b}$$

As discussed in Section 2.3.3, the solar constant derived from recent satellite observations is 1366 W m^{-2}. Inserting the solar constant and global albedo values into the balanced equation, we find $T_e \sim 255$ K. The temperature profile as shown in Fig. 3.1 ranges from about 200 to 300 K.

From Planck's and Wien's displacement laws discussed in Chapter 1, the emitted Planck intensity (or radiance) from the earth and the atmosphere is smaller than that

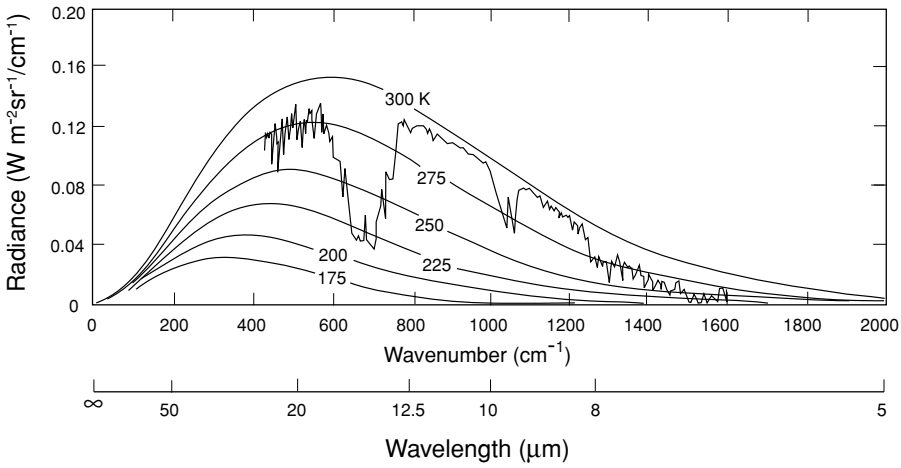

Figure 4.1 Theoretical Planck radiance curves for a number of the earth's atmospheric temperatures as a function of wavenumber and wavelength. Also shown is a thermal infrared emission spectrum observed from the Nimbus 4 satellite based on an infrared interferometer spectrometer.

of solar radiation, whereas the wavelength for the intensity peak of the earth's radiation field is longer than that of solar radiation. The energy emitted from the earth–atmosphere system is also referred to as *thermal IR* or *terrestrial radiation*. The spectral distribution of radiance emitted by a blackbody source at various temperatures in the earth's atmosphere in terms of wavenumber as well as wavelength is displayed in Fig. 4.1, where a measured atmospheric emission spectrum obtained from the infrared interferometer spectrometer (IRIS) instrument on board the Nimbus 4 satellite is also shown. The envelope of the emission spectrum is very close to the spectrum emitted from a blackbody with a temperature of about 290 K, which is about the temperature of the surface. It is evident that a large portion of thermal infrared energy is trapped by various gases in the atmosphere.

Among these gases, carbon dioxide, water vapor, and ozone are the most important absorbers. Some minor constituents, such as carbon monoxide, nitrous oxide, methane, and nitric oxide, which are not identified in Fig. 4.1, are relatively minor absorbers insofar as the heat budget of the earth–atmosphere system is concerned. Carbon dioxide absorbs a significant amount of thermal infrared radiation in the 15 μm band from about 600 to 800 cm^{-1}. This spectral region also corresponds to the maximum intensity of the Planck function in the wavenumber domain. Water vapor absorbs thermal infrared in the 6.3 μm band from about 1200 to 2000 cm^{-1} and in the rotational band (<500 cm^{-1}). Except for ozone, which has an absorption band in the 9.6 μm region, the atmosphere is relatively transparent from 800 to 1200 cm^{-1}. This region is referred to as the *atmospheric window*. As discussed in Section 3.1.2, the distribution of carbon dioxide is fairly uniform over the global space, although there has been observational evidence indicating a continuous global increase over the past century as a result of the increase in combustion of fossil fuels. This

leads to the question of possible changes in the earth's climate due to the increasing concentration of carbon dioxide (Section 8.4.1). Unlike carbon dioxide, however, water vapor and ozone are highly variable with respect to both time and geographical location.

In a clear atmosphere without clouds or aerosols, a large portion (about 50%) of solar energy transmits through the atmosphere and is absorbed by the earth's surface (see Fig. 3.9). In contrast, energy emitted from the earth is largely absorbed by carbon dioxide, water vapor, ozone, and other trace gases in the atmosphere as shown in Fig. 4.1. The trapping of thermal infrared radiation by atmospheric gases is typical of the atmosphere and is therefore called the *atmospheric effect*. It is also referred to as the *greenhouse effect* because of the similar way in which the glass covering of a greenhouse transmits solar radiation but absorbs emitted thermal infrared radiation. The climatological surface temperature is about 288 K. We may express the surface temperature in terms of the equilibrium temperature in the form

$$T_s = T_e + \gamma H, \tag{4.1.2}$$

where γ is the lapse rate and H is defined as the effective height of the greenhouse effect. Based on the standard lapse rate of 6.5 K km^{-1}, H is about 5 km.

A final note is in order. Solar radiation is also called *shortwave radiation* because solar energy is concentrated in shorter wavelengths with its peak at about 0.5 μm. Thermal infrared radiation emitted from the earth and the atmosphere is also referred to as *outgoing longwave radiation* (OLR) because its maximum energy is in the longer wavelengths at about 10 μm. The solar and infrared spectra are separated into two spectral ranges above and below about 5 μm, and the overlap between them is relatively small. This distinction makes it possible to treat the two types of radiative transfer and source functions separately and thereby simplify the complexity of the radiative transfer problem.

Following a discussion of the general characteristics of the vibrational–rotational spectra of water vapor, carbon dioxide, ozone and other minor gases, we present the fundamental theory of infrared radiative transfer and the line-by-line method for the numerical calculations involved. Next, we introduce approximate methods for infrared radiative transfer calculation, including the correlated k-distribution, band model, and broadband emissivity techniques. The subject of infrared radiative transfer in cloudy atmospheres is also further discussed. Finally, typical results of infrared heating and cooling rate profiles in both clear and cloudy atmospheres are presented.

4.2 Absorption and Emission in the Atmosphere

4.2.1 Absorption in the Thermal Infrared

4.2.1.1 Water Vapor

Following the discussion in the subsection on water vapor in Section 3.2.3, the pure H_2O rotational band ranges from 0 to 1000 cm^{-1}. This band is important in

the generation of tropospheric cooling. The ν_2 fundamental band at 1594.78 cm^{-1} (6.25 μm) is the most important vibrational–rotational band of water vapor. The two other fundamental bands, ν_1 and ν_3, are found to be close to one another and are centered at 2.7 μm. The H_2O isotopes $HH^{18}O$, $HH^{17}O$, and $HD^{16}O$ have been identified in both the rotational and ν_2 bands.

The region from 800 to 1200 cm^{-1}, the thermal infrared window, contains the moderately strong 9.6 μm band of ozone discussed later. Apart from the ozone band, absorption is continuous and is primarily due to the water vapor species. The attenuation due to the water vapor continuum in the 10 μm window remains a theoretical mystery. It has been suggested that the continuum results from the accumulated absorption of the distant wings of water vapor lines, principally in the far-infrared part of the spectrum. This absorption is caused by the collision broadening between absorbing molecules (H_2O–H_2O) and between absorbing and nonabsorbing molecules (H_2O–N_2). There is some evidence that contributions to continuous absorption may be caused by water dimer [($H_2O \cdot H_2O$)]. Absorption by water dimer depends significantly on water vapor pressure and temperature. Although accurate and well-controlled measurements are required in order to account for the water vapor continuum in real atmospheric situations, limited experimental measurements have been used to develop empirical parameterizations.

4.2.1.2 Carbon Dioxide

As discussed in Subsection 3.2.3.3, the bending mode, ν_2, is degenerate and consists of ν_{2a} and ν_{2b} vibrations at the same frequency. The CO_2 15 μm band represents this particular vibration. Owing to perpendicular vibration, the ν_2 fundamental transition is coupled with rotational transitions corresponding to changes in the quantum number $\Delta J = -1, 0, +1$. The spectral lines produced by these changes are referred to as the P, Q, and R branches, respectively, as noted in Section 1.3.1. For the P and R branches, the lines have wavenumbers lower and greater, respectively, than those of the line center. In the case of the Q branch, the lines are clustered near the center of the 15 μm band.

Because of the two vibrational modes, ν_{2a} and ν_{2b}, a $\pi/2$ phase difference is produced between them. The central carbon atom will perform a rotary motion about the symmetry axis and generate a component of angular momentum along this axis. This momentum is quantized with a quantum number l that is less than or equal to ν_2. This quantum number is added as a superscript to ν_2 in the designation of the vibrational level, e.g., 01^10, 02^00, 02^20. The $2\nu_2$ level of the carbon dioxide molecule lies very close to the ν_1 level, causing a resonance referred to as *Fermi resonance*. Because of the selection rules on the vibrational angular momentum, only the level 02^00 can combine with ν_1.

Besides the ν_2 fundamental band, numerous combination bands have been detected in the 15 μm region. Simultaneous transitions in two of the vibration modes are possible, resulting in weak combination (or difference) frequencies. There are also numerous hot bands in the 15 μm CO_2 band. These bands are produced by transitions between excited levels and are significant in cooling-rate calculations in the middle

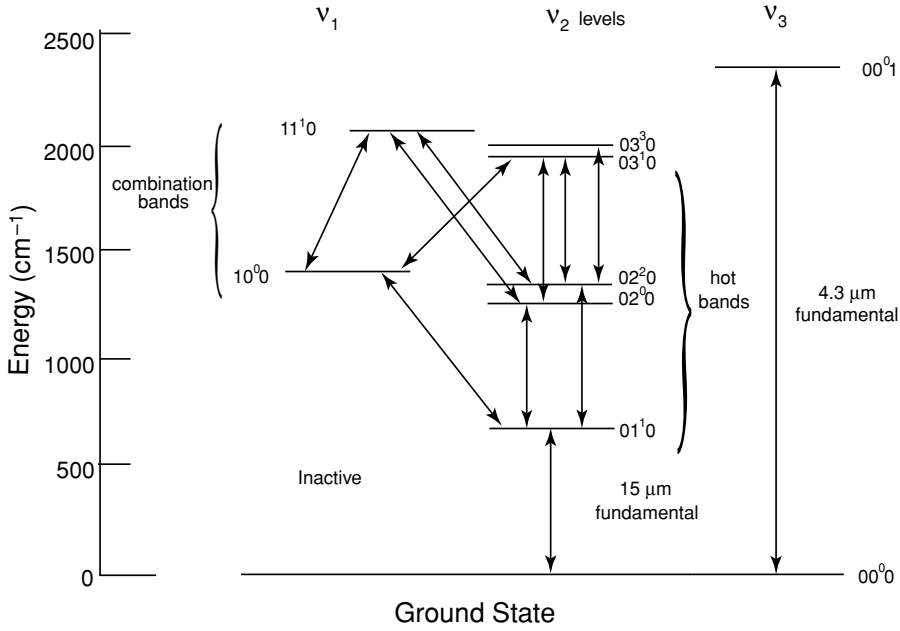

Figure 4.2 The most important vibrational transitions that produce the 15 μm CO_2 band, including the ν_2 fundamental, the hot bands, and the combination bands (data taken from Lopez-Puertas *et al.,* 1986). The rotational bands in this vibrational mode are the $P(\Delta J = -1)$, $Q(\Delta J = 0)$, and $R(\Delta J = +1)$ branches. The isotopes include $^{16}O^{12}C^{16}O$, $^{16}O^{13}C^{16}O$, and $^{16}O^{12}C^{18}O$.

atmosphere. A summary diagram of the 15 μm CO_2 energy transitions is presented in Fig. 4.2.

There are several overtone and combination bands of carbon dioxide in the IR. At atmospheric temperatures, most of the molecular population is in the vibrational level with quantum number $\upsilon = 0$. When transitions take place between nonadjacent levels ($\Delta\upsilon = 2, 3, 4$), weaker overtone frequencies are produced. Two moderately strong bands appear in the solar spectrum and are centered at 1063.8 and 961.0 cm^{-1}. Both are parallel bands and have been used for the development of the CO_2 laser emission at about 10.6 μm. The bands near 5 μm consist of the $3\nu_2$ band at 5.2 μm and several combination bands at 4.8 μm.

4.2.1.3 Ozone

The ozone molecule has an asymmetric top configuration similar to the water vapor molecule, but with a different apical angle, giving it a relatively strong rotational spectrum. The three isotopes, $^{16}O_3$, $^{16}O^{18}O^{16}O$, and $^{16}O^{16}O^{18}O$, have fundamental bands in the 9.6 and 14.27 μm regions. The ν_1 and ν_3 fundamental vibration modes are centered at 1110 and 1043 cm^{-1} and constitute the well-known 9.6 μm ozone band. The ν_2 fundamental band, centered at 705 cm^{-1} (14.27 μm), is well-masked

by the strong CO_2 15 μm band and appears to be less significant in atmospheric radiative transfer. There is also a relatively strong band of ozone at 4.75 μm that is produced by overtone and combination transitions. The electronic bands of ozone were discussed in Section 3.2.1.

4.2.1.4 Methane

The methane molecule has a spherical top configuration. It has no permanent electric dipole moment and, hence, no pure rotational spectrum. There are four fundamental vibration modes. Of these, only ν_3 and ν_4, centered at 3020.3 and 1306.2 cm^{-1}, are active in the infrared spectrum. The ν_4 fundamental band of CH_4 is important in the climatic greenhouse effect. The inactive ν_1 and ν_2 fundamental bands are centered at 2914.2 and 1526 cm^{-1}. Methane also possesses a rich spectrum of overtone and combination bands that have been identified in the solar spectrum.

4.2.1.5 Nitrous Oxide

The nitrous oxide molecule has a linear and asymmetric structure, with the configuration NNO. Similar to carbon dioxide, it has a single rotational constant and a detectable rotational spectrum. Numerous bands produced by the fundamental, overtone, and combination frequencies exist in the infrared. The three fundamental frequencies are centered at 1285.6 cm^{-1}(ν_1), 588.8 cm^{-1} (ν_2), and 2223.5 cm^{-1}(ν_3). The ν_1 fundamental band of nitrous oxide overlaps the ν_4 fundamental band of methane.

4.2.1.6 Chlorofluorocarbons

The methyl chloride (CH_3Cl) molecule has two bands of interest to atmospheric infrared radiative transfer: the ν_3 band at 732 cm^{-1} and the ν_2 band at 1350 cm^{-1}. In the ν_8 region, which is centered at 1161 cm^{-1} and has a band at 1095 cm^{-1}, Q branch features have been found for dichlorodifluoromethane (CF_2Cl_2). For the trichlorofluoromethane ($CFCl_3$) molecule, the ν_1 and ν_4 fundamental transitions are active and centered at 848 and 1085 cm^{-1}, respectively. The methylchloroform (CH_3CC1_3) molecule has a narrow Q branch associated with the ν_2 fundamental band at 1348.5 cm^{-1}. The carbon tetrachloride (CCl_4) molecule has an active band in the ν_3 region near 796 cm^{-1}. Absorption of these anthropogenic trace gases is primarily located in the window region. Thus, their potential increase can make the atmospheric window "dirty" and may lead to significant greenhouse effects.

All the preceding absorbing gases are identified in the infrared spectrum presented in Fig. 4.3, obtained from a scanning high-resolution interferometer sounder (S-HIS; see also Fig. 4.12), an instrument that measures the emitted thermal radiation between 3.3 and 18 μm from the NASA high-flying ER-2 aircraft at about 20 km. The spectral resolution of this interferometer varies but is on the order of 0.01 cm^{-1}. The spectrum is presented in terms of the brightness temperature (see Section 7.5.1 for the conversion of radiance to brightness temperature). Note that in addition to the absorption of the 4.3 μm CO_2 band (Section 3.2.3) in the solar spectral region of 3.3 to 5.0 μm, the absorption of nitrogen species is also identified.

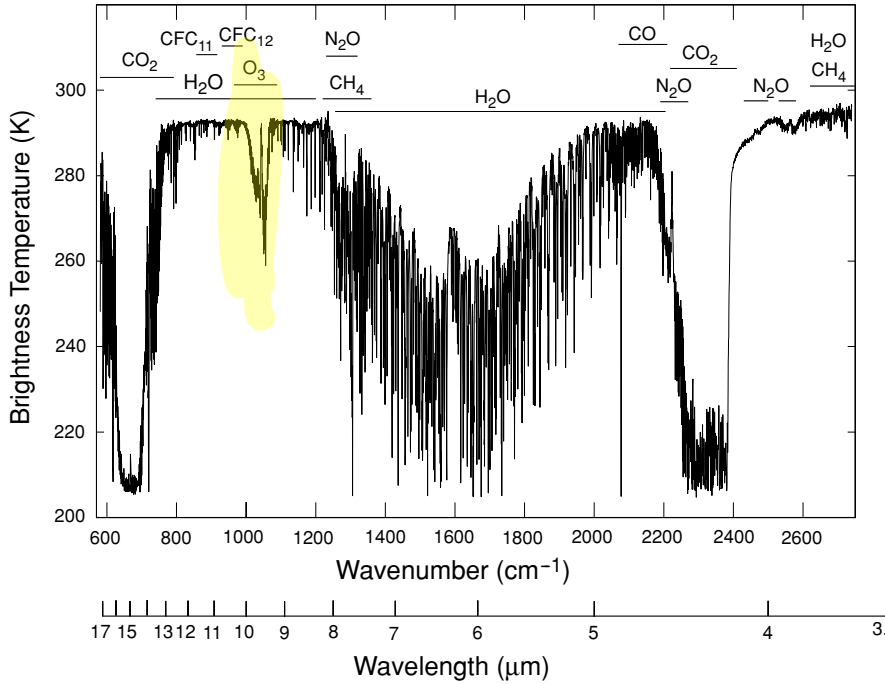

Figure 4.3 Observed infrared spectrum displaying all the absorption gases and their spectral location. This spectrum was obtained from the scanning high-resolution interferometer sounder (S-HIS), which measured the emitted thermal radiation between 3.3 and 18 μm, onboard the NASA ER-2 aircraft over the Gulf of Mexico southeast of Louisiana on April 1, 2001 (courtesy of Allen Huang and Dave Tobin of the University of Wisconsin).

4.2.2 Fundamentals of Thermal Infrared Radiative Transfer

Consider an absorbing and emitting medium. A pencil of radiation traversing this medium will be weakened by the interaction with matter through absorption. At the same time, this radiation may be strengthened by thermal emission from the medium (see Section 1.4.3). This pencil of radiation is usually represented by its intensity (or radiance), I_ν, in the field of radiative transfer. The general equation for radiative transfer in an absorbing and emitting medium can be written in terms of the differential change in the intensity in the form

$$-\frac{1}{k_\nu \rho_a}\frac{dI_\nu}{ds} = I_\nu - J_\nu, \tag{4.2.1}$$

where k_ν denotes the absorption coefficient, ρ_a is the density of absorbing gases, s is the slant path, and J_ν is the source function. For applications concerning the radiation budget of the planet, it suffices to consider the intensity as being independent of time. Moreover, it is commonly assumed that, in localized portions, the atmosphere is in thermodynamic equilibrium, as well as being plane-parallel. The first

assumption allows us to use the Planck intensity for the source function by virtue of Kirchhoff's law. The plane-parallel assumption implies that variations in the intensity and atmospheric parameters (temperature and gaseous profiles) are permitted only in the vertical direction (e.g., height or pressure). Under this assumption, absorption and emission processes would be symmetrical with respect to the azimuthal angle. It follows that the intensity is a function of the vertical position and zenith angle. Under these conditions, the basic equation that governs thermal IR radiation in the height coordinate may be written in the form

$$-\mu \frac{dI_\nu(z,\mu)}{k_\nu \rho_a dz} = I_\nu(z,\mu) - B_\nu(z), \tag{4.2.2}$$

where the Planck intensity $B_\nu(z) = B_\nu(T(z))$.

Because of the height dependence of both the gaseous density and absorption coefficient, it is convenient to define the *normal optical depth,* or simply *optical depth,* in the form

$$\tau = \int_z^{z_\infty} k_\nu(z')\rho_a(z')dz' = \int_0^p k_\nu(p')q(p')\frac{dp'}{g}, \tag{4.2.3}$$

where z_∞ denotes the height at the top of the atmosphere (TOA), $q = \rho_a/\rho$, the gaseous mixing ratio, and ρ is the air density. We have introduced the pressure coordinate p, using the hydrostatic equation. Figure 4.4 shows the coordinate systems in optical depth, height, and pressure. The differential optical depth can be readily obtained from Eq. (4.2.3) with the form $d\tau = -k_\nu(z)\rho_a(z)dz = k_\nu(p)q(p)dp/g$. In

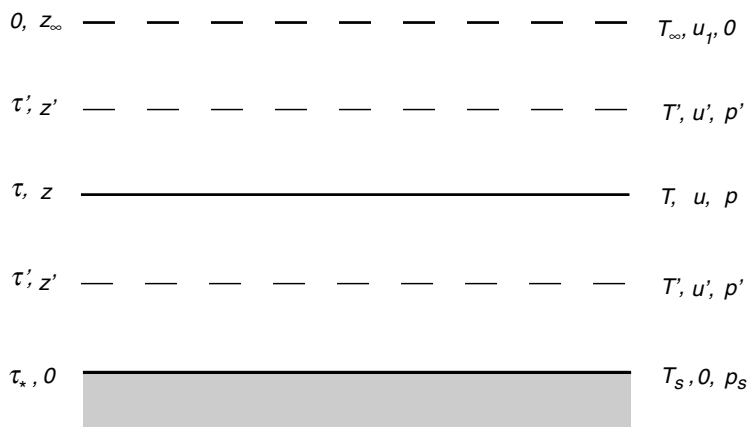

Figure 4.4 Coordinate systems in τ, z, u, T, and p for IR radiative transfer in plane-parallel atmospheres. u is the path length for absorbing gases defined from the surface upward. The total path length is denoted by u_1. T_∞ and z_∞ are temperature and height, respectively, at TOA. The surface temperature $T_s = T(\tau_*)$. The surface pressure is denoted by p_s.

terms of the τ coordinate, Eq. (4.2.2) may be rewritten as follows:

$$\mu \frac{dI_\nu(\tau, \mu)}{d\tau} = I_\nu(\tau, \mu) - B_\nu(\tau). \tag{4.2.4}$$

For the upward intensity, the zenith angle $0 \le \theta \le \pi/2$; that is, $0 \le \mu \le 1$. However, for the downward intensity, $\pi/2 \le \theta \le \pi$. In this case, we may set $\mu = -\mu$ for convenience in radiative transfer analyses.

Equation (4.2.4) represents a first-order differential equation. In order to solve both upward and downward components for an atmosphere with a total optical depth of τ_*, two boundary conditions are required. Under the plane-parallel assumption, these conditions are isotropic emissions from both the surface and TOA. In general, the earth's surface may be considered as a blackbody in the infrared, so that $I_\nu(\tau_*, \mu) = B_\nu(T(\tau_*))$. In addition, we may allow for a possible source of downward emission at TOA and write $I_\nu(0, -\mu) = B_\nu(\text{TOA})$. Normally, however, $B_\nu(\text{TOA}) \cong 0$. Subject to the preceding boundary conditions, the formal solutions for upward and downward intensities are given by

$$I_\nu^{\uparrow}(\tau, \mu) = B_\nu(\tau_*)e^{-(\tau_* - \tau)/\mu} + \int_\tau^{\tau_*} B_\nu(\tau')e^{-(\tau' - \tau)/\mu} \frac{d\tau'}{\mu}, \tag{4.2.5a}$$

$$I_\nu^{\downarrow}(\tau, -\mu) = \int_0^{\tau} B_\nu(\tau')e^{-(\tau - \tau')/\mu} \frac{d\tau'}{\mu}. \tag{4.2.5b}$$

We shall now define the *monochromatic transmittance* (also referred to as the *transmission function*) so that the exponential attenuation may be expressed by

$$T_\nu(\tau/\mu) = e^{-\tau/\mu}. \tag{4.2.6a}$$

The differential form is

$$\frac{dT_\nu(\tau/\mu)}{d\tau} = \frac{-1}{\mu} e^{-\tau/\mu}. \tag{4.2.6b}$$

The formal solutions for the intensities can then be expressed by

$$I_\nu^{\uparrow}(\tau, \mu) = B_\nu(\tau_*)T_\nu[(\tau_* - \tau)/\mu] - \int_\tau^{\tau_*} B_\nu(\tau') \frac{d}{d\tau'} T_\nu[(\tau' - \tau)/\mu]\, d\tau', \tag{4.2.7a}$$

$$I_\nu^{\downarrow}(\tau, -\mu) = \int_0^{\tau} B_\nu(\tau') \frac{d}{d\tau'} T_\nu[(\tau - \tau')/\mu]\, d\tau'. \tag{4.2.7b}$$

Equation (4.2.7a) can be applied to remote sensing from space if we set $\tau(\text{TOA}) = 0$.

For atmospheric heating rate calculations, the required quantities are the upward and downward flux densities (simply referred to as fluxes hereafter), which are the sum of the directional intensities from the upper and lower hemispheres, respectively. In accordance with the plane-parallel assumption, we have

$$F_\nu^{\uparrow\downarrow}(\tau) = 2\pi \int_0^1 I_\nu^{\uparrow\downarrow}(\tau, \pm\mu)\mu\, d\mu. \tag{4.2.8}$$

On noting the angular integration and in order to obtain the fluxes, we may define a physical parameter, referred to as *slab* or *diffuse transmittance,* in the form

$$T_\nu^f(\tau) = 2\int_0^1 T_\nu(\tau/\mu)\mu\, d\mu. \tag{4.2.9}$$

With the aid of this definition, the expressions for fluxes may now be written in the form

$$F_\nu^\uparrow(\tau) = \pi B_\nu(\tau_*)T_\nu^f(\tau_* - \tau) - \int_\tau^{\tau_*} \pi B_\nu(\tau')\frac{d}{d\tau'}T_\nu^f(\tau' - \tau)\, d\tau', \tag{4.2.10a}$$

$$F_\nu^\downarrow(\tau) = \int_0^\tau \pi B_\nu(\tau')\frac{d}{d\tau'}T_\nu^f(\tau - \tau')\, d\tau'. \tag{4.2.10b}$$

The upward flux at a given level comes from two sources: the surface emission that is attenuated to that level and the emission contributions from the atmospheric layers characterized by Planck fluxes multiplied by the weighting function, $dT_\nu^f/d\tau$. Likewise, the downward flux at a given level is produced by the contributions from the atmospheric layers.

Finally, to account for the contributions from all wavenumbers in the thermal IR spectrum, an integration of the monochromatic flux with respect to wavenumber must be performed. Since τ is a function of the wavenumber, we use the height coordinate and write

$$F^{\uparrow\downarrow}(z) = \int_0^\infty F_\nu^{\uparrow\downarrow}(z)\, d\nu. \tag{4.2.11}$$

At this point, the transfer of thermal IR radiation in plane-parallel atmospheres (without clouds) is formally solved. Conditional to the definition of diffuse transmittance, the computation of atmospheric fluxes involves solving the integrations over the wavenumber and along the optical depth.

4.2.3 Line-By-Line (LBL) Integration

Absorption line parameters for various gases can be computed from fundamental quantum mechanics theory. Laboratory data are also available for a limited number of spectral intervals. Based on theory and measurements, line parameters have been compiled over the range 0 to 17,900 cm^{-1} (Rothman *et al.,* 1998). Data for more than 1 million lines have been presented. The absorption line parameters are listed in data form in terms of line position (in cm^{-1}), line intensity [in cm^{-1}/(mol cm^{-2}) at 296 K], air-broadened half-width (in cm^{-1}/atm at 296 K), and lower-state energy (in cm^{-1}). The molecular species include H_2O, CO_2, O_3, N_2O, CO, CH_4, and O_2.

For a given wavenumber and species, contributions to transmittance arise from the absorption coefficients for N lines. The optical depth is then

$$\tau = \sum_{j=1}^N \tau_j = \int_u \sum_{j=1}^N k_{\nu,j}(u)\, du, \tag{4.2.12}$$

where $j(= 1, 2, \ldots, N)$ is the index of the absorption coefficient for the jth line. Thus, the absorption coefficient can be expressed in terms of line strength and line shape in the form

$$k_\nu(p, T) = \sum_{j=1}^{N} S_j(T) f_{\nu,j}(p, T). \tag{4.2.13}$$

In order to resolve individual lines, the absorption coefficient must be computed at wavenumber intervals that are smaller than the line half-width. In the upper stratosphere, absorption and emission processes are dominated by CO_2 and O_3. Broadening of the absorption lines is primarily due to the Doppler effect. The Doppler half-width in the 15 μm CO_2 and 9.6 μm O_3 bands is $\sim$0.0005–0.001 cm^{-1}. The spectral interval in these two bands covers about 400 cm^{-1}. Thus, the absorption must be calculated at more than half a million points if individual lines are to be resolved.

In the troposphere, absorption due to H_2O predominates. H_2O lines cover essentially the entire infrared spectrum with a spectral region of about 15,000 cm^{-1}. These lines are broadened by collisions, and their half-widths are $>$0.01 cm^{-1}. Computations must be performed at about 1 million points to resolve H_2O lines. For each point, there are numerous lines and atmospheric conditions that must be considered for applications to atmospheric radiative transfer. The computer time required for line-by-line calculations, even with the availability of a supercomputer, is formidable. This is especially true for flux calculations in which an integration over all absorption bands is necessary.

In the case of Lorentz line shapes, it is important to cut off the contribution of significant lines at computational points in a line-by-line program. The far wings of a pressure-broadened absorption line in the infrared have been suggested to be sub-Lorentzian. Two approaches have been used to compute the far wing contribution. The first approach is to multiply the Lorentz profile by an empirical function χ, such that $\chi = 1$ at the line center and $\chi = 0$ at some distance from the center. The second is to use the Lorentz profile for all wavenumbers but to cut the lines off at some distance from the line center. The lines can be cut off at a constant distance from the center or they can be cut off at a distance varying with the half-width; that is, the cutoff wavenumber $\nu_c = \beta\alpha$, with β a constant. Numerical computations show that absorption is affected only slightly by cutting a line off at a wavenumber of about 200 times the Lorentz half-width from the center.

In infrared radiative transfer calculations, it is advantageous to define the radiative parameters in a small spectral interval such that variation of the Planck function can be neglected. In terms of the basic parameters in the intensity and flux equations, we may define the spectral transmittance as

$$T_{\bar{\nu}}(u) = \int_{\Delta\nu} e^{-\tau} \frac{d\nu}{\Delta\nu} = \int_{\Delta\nu} \exp\left(- \int_u \sum_j k_{\nu,j}(u) du \right) \frac{d\nu}{\Delta\nu}. \tag{4.2.14}$$

Thus, in order to calculate the spectral transmittance $T_{\bar{\nu}}(u)$ exactly, adequate and reliable summations must be performed to cover the absorption lines, the spectral

interval, and the nonhomogeneous path. Moreover, the absorption coefficient is a function of the line strength, which is in turn a function of temperature and the half-width, which is itself a function of pressure and temperature. Exact line-by-line calculations for the spectral transmittance are very tedious and require a significant amount of computer time. All the infrared radiative transfer theories that have been developed are essentially intended to simplify and economize the computation of the spectral transmittance by circumventing the integration over the spectral interval and nonhomogeneous path length.

For flux calculations, the diffuse transmittance defined in Eq. (4.2.9) is required. In general, a four-point Gaussian quadrature will give accurate results for integration over the cosine of the zenith angle μ. For many atmospheric applications, it suffices to use

$$T_{\bar{\nu}}^{f}(u) \cong T_{\bar{\nu}}(u/\bar{\mu}), \tag{4.2.15}$$

where $1/\bar{\mu}$, the inverse of the mean emergent angle, is referred to as the *diffusivity factor*. Based on numerical computations for thermal IR radiative transfer, a good approximation for $1/\bar{\mu}$ ranges from 1.66 to 2. The diffusivity of 1.66 was originally proposed by Elsasser (1942) and has been found to be a reliable approximation for the computation of radiative fluxes and heating rates in clear atmospheres. Finally, it should be noted that the notation T is being used in this text as transmittance defined by a wavenumber subscript in infrared radiative transfer discussion, and as the transmission function defined by incoming and outgoing directions in the presentation of multiple scattering processes. It is also being used as temperature throughout the text.

4.3 Correlated K-Distribution Method for Infrared Radiative Transfer

4.3.1 Fundamentals

The k-distribution method for the computation of infrared radiative transfer is based on the grouping of gaseous spectral transmittances according to the absorption coefficient k_ν. In a homogeneous atmosphere, spectral transmittance is independent of the ordering of k for a given spectral interval. Hence, wavenumber integration may be replaced by an integration over the k space. If the normalized probability distribution function for k_ν in the interval $\Delta\nu$ is given by $f(k)$ and its minimum and maximum values are $k_{\min}$ and $k_{\max}$, respectively, then the spectral transmittance may be expressed by

$$T_{\bar{\nu}}(u) = \int_{\Delta\nu} e^{-k_\nu u} \frac{d\nu}{\Delta\nu} = \int_0^\infty e^{-ku} f(k)\, dk, \tag{4.3.1a}$$

where we have set $k_{\min} \to 0$ and $k_{\max} \to \infty$, for mathematical convenience, and

$$\int_0^\infty f(k) dk = 1. \tag{4.3.1b}$$

From Eq. (4.3.1a), the probability distribution function is the inverse Laplace transform, L^{-1}, of the spectral transmittance such that

$$f(k) = L^{-1}(T_{\bar{\nu}}(u)). \tag{4.3.2}$$

If the spectral transmittance can be expressed in terms of an analytic exponential function and if the inverse Laplace transform can be performed, then an analytic expression can be derived for the probability distribution function (Exercises 4.3 and 4.4).

Moreover, a cumulative probability function may be defined in the form

$$g(k) = \int_0^k f(k)\,dk, \tag{4.3.3}$$

where $g(0) = 0$, $g(k \to \infty) = 1$, and $dg(k) = f(k)\,dk$. By definition, $g(k)$ is a monotonically increasing and smooth function in k space. By using the g function, the spectral transmittance can be written

$$T_{\bar{\nu}}(u) = \int_0^1 e^{-k(g)u} dg \cong \sum_{j=1}^{M} e^{-k(g_j)u} \Delta g_j. \tag{4.3.4}$$

From Eq. (4.3.3), since $g(k)$ is a smooth function in k space, the inverse will also be true here; that is, $k(g)$ is a smooth function in g space. Consequently, the integration in g space, which replaces the tedious wavenumber integration, can be evaluated by a finite sum of exponential terms, as shown in Eq. (4.3.4).

Figure 4.5a shows k_ν as a function of ν in a portion of the H_2O rotational band at a pressure of 600 mb and a temperature of 260 K. Figure 4.5b shows the probability distribution $f(k)$ as a function of k for this band [see the following for an evaluation of $f(k)$]. In Fig. 4.5c, the cumulative probability function $g(k)$ is shown as a function of k. We may then compute $k(g)$ as a function of g from Eq. (4.3.3). This curve is illustrated in Fig. 4.5d. Since g is a smooth monotonic function, a few quadrature points will suffice to achieve a high degree of accuracy in the transmittance computation. The physical foundation for the k distribution is quite simple, but it offers an advantage in the computation of infrared flux transfer. The idea of scrambling and ranking absorption lines was described in Ambartzumian's (1936) work on the equilibrium temperature of stellar atmospheres. Arking and Grossman (1972) used this method to discuss the line shape effect on the temperature of planetary atmospheres.

4.3.2 Application to Nonhomogeneous Atmospheres

The preceding theory of the k-distribution method assumes that the absorption coefficient is constant so that ν-integration can be replaced by g-integration. However, as pointed out in Section 4.2.3, the absorption coefficient varies greatly with pressure and temperature in terms of its half-width and line strength. Thus, in order to apply the k-distribution method to realistic atmospheres, variation in the absorption coefficient in the vertical must be accounted for. Basically, we must determine whether the

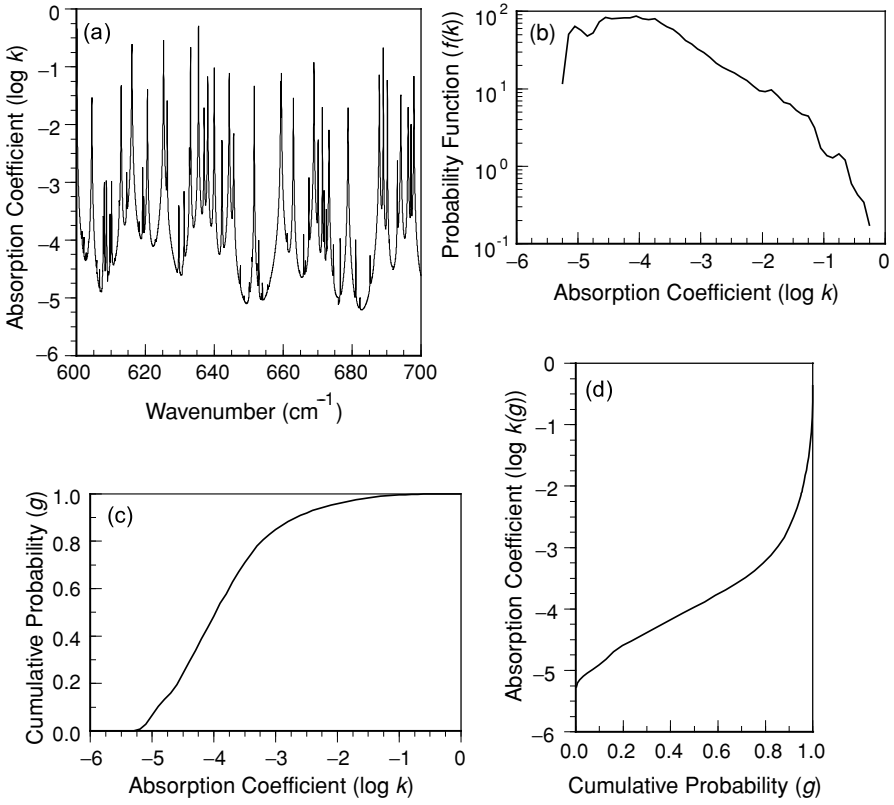

Figure 4.5 (a) Absorption coefficient k_ν in units of (cm atm)$^{-1}$ as a function of wavenumber with a resolution of 0.01 cm^{-1} in the H_2O rotational band with $p = 600$ mb and $T = 260$ K. (b) The probability function $f(k)$ of the absorption coefficient. (c) The cumulative probability function for $f(k)$ shown in (b), plotted as a function of k. (d) Same as (c), except that values of the absorption coefficient are expressed as a function of g.

following two integrations are equivalent:

$$T_{\bar{\nu}}(u) = \int_{\Delta\nu} \exp\left(-\int_u k_\nu \, du\right) \frac{d\nu}{\Delta\nu} \stackrel{?}{\equiv} \int_0^1 \exp\left[-\int_u k(g)\, du\right] dg. \tag{4.3.5}$$

Because the line profile varies significantly from one pressure (temperature) level to another, the rearrangement of all the lines so that the ν- and g-integrations are the same is not obvious. The method that assumes the two are equivalent is referred to as the correlated k-distribution (CKD) method. In the following, we examine the conditions under which the CKD method may be considered to be exact.

Consider first a single line of any shape in a spectral interval $\Delta\nu$. Let this interval be from $-\Delta\nu/2$ to $+\Delta\nu/2$. At the line center, $\nu(k_{\max}) = 0$ and at the end of the line $|\nu(k_{\min})| = \Delta\nu/2$, as shown in Fig. 4.6a. The cumulative probability function defined

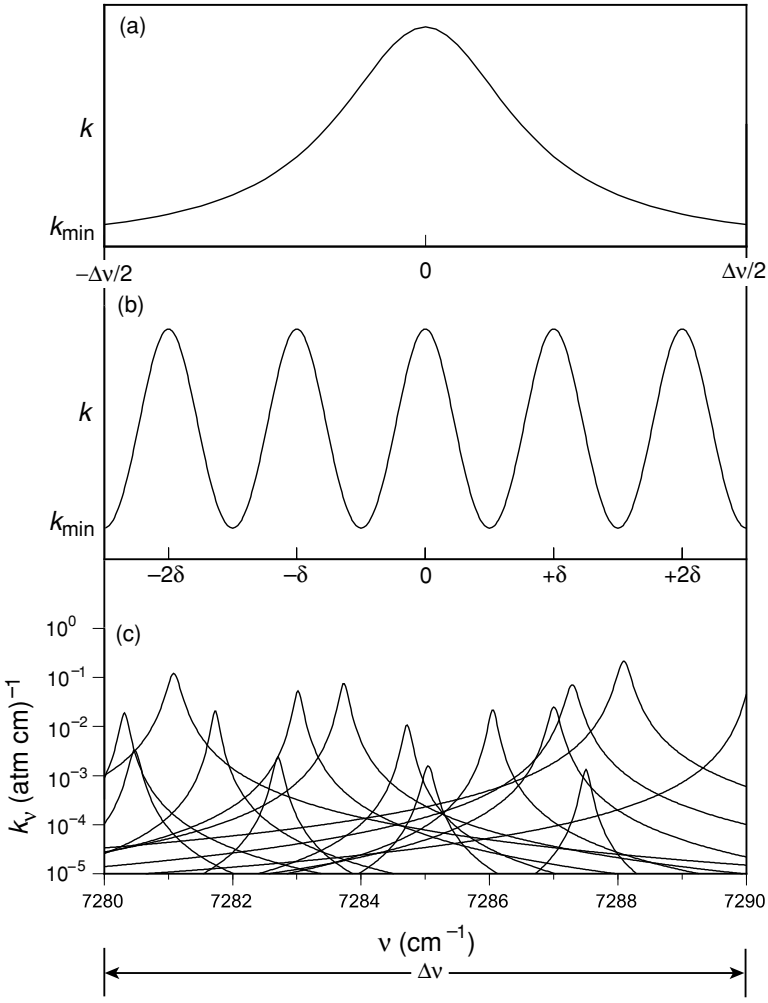

Figure 4.6 (a) A single line, (b) periodic (regular) lines where δ is the line spacing, and (c) Lorentz lines in a 10 cm^{-1} interval in the 1.38 μm H_2O band. Fifteen lines are shown.

in Eq. (4.3.3) is given by

$$g(k) = \frac{2}{\Delta\nu}\int_{k_{\min}}^{k}\left|\frac{d\nu}{dk}\right|_{k=k'} dk' = \frac{2}{\Delta\nu}\nu(k) - 1. \tag{4.3.6a}$$

It follows that $(2/\Delta\nu)\,d\nu = dg$. That is, for a single line, we can replace the integration over the ν-domain with an integration over the g-domain in Eq. (4.3.5). Consider now a group of n lines that occur periodically (or regularly) in a spectral interval $\Delta\nu$

(Fig. 4.6b). Let the line spacing be δ. Then we have

$$g(k) = \frac{2}{\delta}\int_{k_{\min}}^{k}\left|\frac{d\nu}{dk}\right|_{k=k'} dk' = \frac{2}{\delta}\nu(k) - 1. \tag{4.3.6b}$$

Thus, $(2/\delta)\,d\nu = dg$. Again, the integration over the ν-domain can be replaced by an integration over the g-domain. Calculations of the spectral transmittance would be the same in the two approaches. For reference purposes, Fig. 4.6c shows a group of absorption lines assuming the Lorentz shape in a 10 cm^{-1} spectral interval within the 1.38 μm H_2O band.

Next, if the absorption coefficient and/or the path length is small, referred to as the *weak-line limit,* we have from Eq. (4.3.5), regardless of the line shape, the following:

$$T_{\bar{\nu}}(\text{weak}) \cong \int_{\Delta\nu}\left[1 - \int_u k_\nu\, du\right]\frac{d\nu}{\Delta\nu} = 1 - \int_u k_*\, du, \tag{4.3.7a}$$

where $k_* = \sum S_j/\Delta\nu$ and is independent of wavenumber. The last expression is obtained by employing the definition of the absorption coefficient given in Eq. (4.2.13). Since k_* is small, we may rewrite Eq. (4.3.7a) in the form

$$T_{\bar{\nu}}(\text{weak}) = \exp\left(-\int_u k_*\, du\right). \tag{4.3.7b}$$

Under the weak-line limit, the spectral transmittance may be expressed explicitly by an exponential function without integration over ν. This is referred to as the *gray approximation*. In this case, replacement of $d\nu/\Delta\nu$ by dg can readily be made, since k_* is independent of ν.

Now consider a group of lines. The absorption coefficient at a given wavenumber is contributed from all the lines and using the Lorentz profile, we have

$$k_\nu(p, T) = \sum_j \frac{S_j(T)}{\pi}\frac{\alpha_j(p, T)}{(\nu - \nu_0)^2 + \alpha_j^2(p, T)}, \tag{4.3.8}$$

where the line strength is a function of temperature and the half-width is a function of both pressure and temperature [see Eq. (1.3.14)]. At the line center, $\nu = \nu_0$, $k_\nu \sim 1/\alpha_j(p, T) \sim 1/p$. However, in the far wing, $|\nu - \nu_0| \gg \alpha$, and $k_\nu \sim \alpha_j(p, T) \sim p$. Under normal atmospheric conditions, the half-widths of Lorentzian lines are small in comparison to the mean line spacing. This is particularly true for most water vapor lines. Near the line centers, absorption becomes saturated so that the transfer of radiation through the wing regions becomes predominant. This is the condition for the *strong-line limit*. In this case, we may write

$$k_\nu(p, T) \cong \sum_j \frac{S_j(T)}{\pi}\frac{\alpha_j(p, T)}{(\nu - \nu_0)^2} = k_\nu^* f^*(p, T), \tag{4.3.9}$$

where

$$k_\nu^* = 1/\pi(\nu - \nu_0)^2, \quad f^*(p, T) = \sum_j S_j(T)\alpha_j(p, T).$$

The condition in which the dependent variable ν may be separated from the absorption coefficient is referred to as the *scaling approximation*. Substituting Eq. (4.3.9) into Eq. (4.3.5) leads to

$$T_{\bar{\nu}}(\text{strong}) \cong \int_{\Delta\nu} e^{-k_\nu^* \tilde{u}} \frac{d\nu}{\Delta\nu} \equiv \int_0^1 e^{-k_\nu^*(g)\tilde{u}} dg, \tag{4.3.10}$$

as in the homogeneous case, where

$$\tilde{u} = \int_u f^*(p, T)\, du.$$

In essence, the scaling approximation allows the transformation of a nonhomogeneous path into a homogeneous path.

On the basis of the preceding discussion, the CKD method is exact for a single line and periodic lines, as well as in the limits of weak-line and strong-line approximations. The CKD method is an extension of the k-distribution to nonhomogeneous paths, the idea of which appeared in a technical report (Lacis *et al.,* 1979). In this method, the vertical nonhomogeneity of the atmosphere is accounted for by assuming a simple correlation of k-distributions at different temperatures and pressures such that the spectral transmittance can be expressed by

$$T_{\bar{\nu}}(u) \cong \int_0^1 \exp\left[-\sum_i k_i(g)\Delta u_i \right] dg. \tag{4.3.10}$$

Because the CKD approach allows the use of k-distributions at each altitude, an appropriate Voigt profile can also be accounted for throughout the atmosphere. Moreover, it can also be used for absorption bands in both solar and thermal infrared spectra and, at the same time, the results from this method can be directly incorporated into multiple-scattering processes associated with cloud and aerosol particles. Goody *et al.* (1989), Lacis and Oinas (1991), and Fu and Liou (1992) have undertaken proof of the validity of CKD and have tested its accuracy under a variety of atmospheric conditions. For flux calculations, errors due to the assumptions in CKD with respect to LBL results are generally on the order of 1%. Thus, the CKD method is a powerful technique for use in radiative transfer parameterizations in dynamic and climate models especially when multiple scattering of cloud and aerosol particles must be accounted for in flux and heating rate calculations. The accuracy of CKD will be further elaborated upon in Section 4.7. In the following, we discuss a simple numerical procedure for the sorting of absorption lines.

4.3.3 Numerical Procedures and Pertinent Results

Consider a spectral interval $\Delta\nu$ that contains numerous absorption lines. We may divide this interval into a subset of $\Delta\nu_i (i = 1, 2 \ldots, N)$ such that they are less than the line's half-width. In this case, the probability distribution function may be

written as

$$f(k) = \frac{1}{\Delta\nu}\frac{d\nu}{dk} = \frac{1}{\Delta\nu}\sum_j \left|\frac{\Delta\nu_j}{\Delta k}\right| \tag{4.3.11}$$

for a specific k, and $f(k)$ is 0 if the maximum of a line k_j (max) is smaller than k. The cumulative probability function is then

$$\begin{aligned} g(k) &= \frac{1}{\Delta\nu}\sum_j \int_0^k \left|\frac{\Delta\nu_j}{\Delta k'}\right| dk' \\ &= \frac{1}{\Delta\nu}\sum_j \int_0^k \Delta\nu_j(k) = \frac{n(0,k)}{N}, \end{aligned} \tag{4.3.12}$$

where the total number of lines (computational points) $N = \Delta\nu/\delta$, with δ the mean line spacing defined by

$$\delta = \sum_{j=1}^{N} \nu_j/N, \tag{4.3.13}$$

and $n(0, k)$ denotes the number of lines (computational points) that contribute to k cumulatively.

For illustration purposes, let us consider three lines as displayed in Fig. 4.7. We may divide the absorption coefficient into 10 intervals. As shown, $n(0, \Delta k) = 4$, $n(0, 2\Delta k) = 4 + 6 = 10$, and so on. The total number $N = n(0, 9\Delta k) = 35$. From Eq. (4.3.12), we have $g(0) = 0$, $g(\Delta k) = 4/35$, $g(2\Delta k) = 10/35, \ldots$, and $g(9\Delta k) = 1$. The absorption coefficient $k(g)$ can now be expressed in the g-domain, as shown in Fig. 4.7, and is a monotonically increasing function. It follows that the computation of spectral transmittance may now be performed over the g-domain, with a relatively small number of computational points, instead of the ν-domain, which consists of highly fluctuating curves. Exercise 4.1 requires the analysis and computation of the g function and spectral transmittance for a group of water vapor lines in a 10 cm^{-1} spectral interval.

The foregoing procedure can be used to compute g functions for a given pressure and temperature, i.e., $g(k, p, T) = n(0, k; p, T)/N$. The effect of pressure and temperature on the absorption coefficient in the g-domain is shown in Fig. 4.8 using a spectral interval of 540–670 cm^{-1} in the 15 μm CO_2 band. For a given g, the absorption coefficient increases with increasing pressure and temperature. The pressure effect occurs through its dependence on the half-width, whereas the temperature effect is associated with both line strength and half-width. In numerical calculations of IR heating rates, it would be advantageous and practical to develop efficient parameterizations to account for the dependence of pressure and temperature on the absorption coefficient in the g-domain.

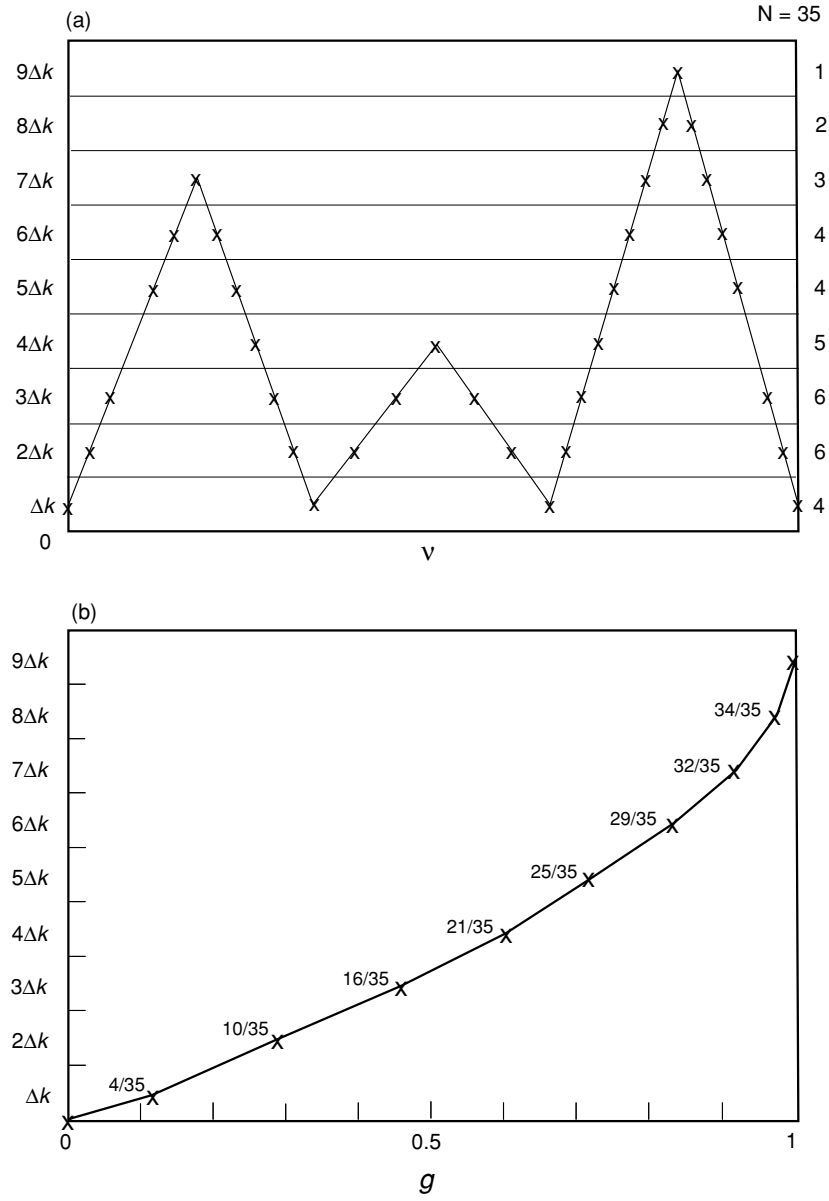

Figure 4.7 Illustration of the mapping of the absorption coefficient from the ν-domain to the g-domain. (a) Absorption coefficients of three lines in the ν-domain and division of the k-space into 10 equal intervals. The numbers are the data points in each interval with a total number of 35. (b) By definition, $g(j\,\Delta k) = n(0, j\,\Delta k)/N$, $j = 0, 1, \ldots, 9$. Thus, the data points in the ν-domain are transformed to the g-domain, where g is a monotonic increasing function.

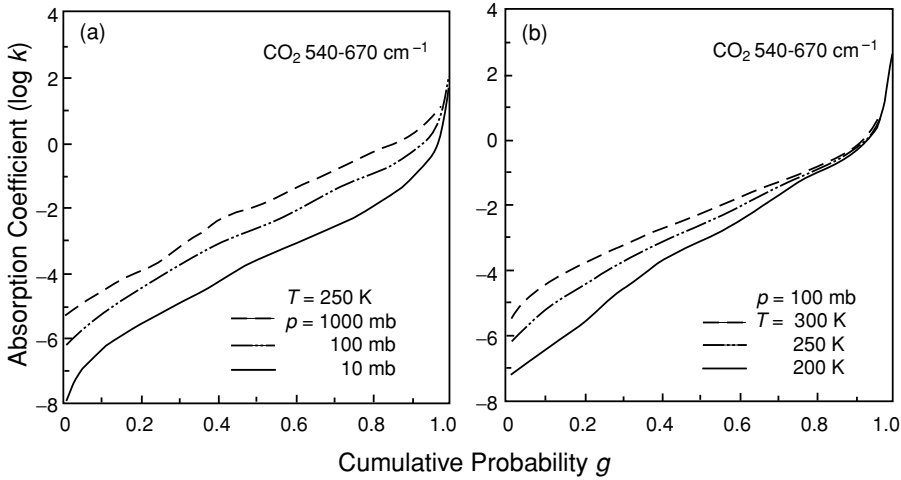

Figure 4.8 The absorption coefficient in (cm atm)$^{-1}$ as a function of the cumulative probability g for the CO_2 540–670 cm^{-1} spectral region (a) for a temperature of 250 K with three pressures and (b) for a pressure of 100 mb with three temperatures.

4.3.4 Line Overlap Consideration

Examination of the line displacement reveals that H_2O rotational lines and a portion of 15 μm CO_2 lines overlap significantly. Thus, an appropriate treatment must be undertaken to evaluate the spectral transmittance that contains the two gases. Let the mixing ratios for CO_2 and H_2O be q_c and q, respectively. Their respective optical depths are, therefore, given by

$$\tau_1 = q_c \int k_1(\nu, p, T)\rho \, dz, \tag{4.3.14a}$$

$$\tau_2 = \int k_2(\nu, p, T) q \rho \, dz, \tag{4.3.14b}$$

where ρ is the air density and q_c is a constant. The monochromatic transmittance for the two gases, by definition, can be written in the form

$$T_\nu(q, q_c) = e^{-(\tau_1+\tau_2)} = T_\nu(q_c)T_\nu(q). \tag{4.3.15}$$

Consider a small spectral interval such that $\Delta\nu \leq 5$ cm^{-1}. The H_2O and CO_2 lines may be treated as statistically independent so that

$$\int_{\Delta\nu} [T_\nu(q) - T_{\bar{\nu}}(q)][T_\nu(q_c) - T_{\bar{\nu}}(q_c)] \frac{d\nu}{\Delta\nu} = 0. \tag{4.3.16}$$

In this case, the spectral transmittance for the two gases is separable, leading to

$$T_{\bar{\nu}}(q, q_c) = T_{\bar{\nu}}(q_c)T_{\bar{\nu}}(q) = \int_{\Delta\nu} e^{-\tau_1} \frac{d\nu}{\Delta\nu} \cdot \int_{\Delta\nu} e^{-\tau_2} \frac{d\nu}{\Delta\nu}. \tag{4.3.17a}$$

We may then apply the CKD method to each gas to obtain

$$T_{\bar{\nu}}(q, q_c) \cong \int_0^1 \int_0^1 \exp\left\{-\int [k(g_1)q_c + k(g_2)q]\rho\, dz\right\} dg_1\, dg_2. \tag{4.3.17b}$$

The spectral transmittance now consists of two integrations. If M and N calculations are required for CO_2 and H_2O separately, then the total number of calculations would be $M \times N$, substantially increasing the computational requirement.

In the following, we wish to find a simplified approach to evaluate the spectral transmittance involving two overlap gases. We shall first consider the homogeneous condition such that the spectral transmittance defined in Eq. (4.3.17a) can be expressed by the definition of the k-distribution in the form

$$T_{\bar{\nu}}(q, q_c) = \int_0^\infty e^{-k_1 u_1} f_1(k_1) dk_1 \cdot \int_0^\infty e^{-k_2 u_2} f_2(k_2)\, dk_2, \tag{4.3.17c}$$

where the path lengths $u_1 = q_c u$ and $u_2 = qu = u_1 q/q_c$, with u being the path length for air. With the definitions of u_1 and u_2, the two individual spectral transmittances can then be written as

$$T_{\bar{\nu}}(q_c) = T_1(u_1) = \int_0^\infty e^{-k_1 u_1} f_1(k_1)\, dk_1, \tag{4.3.18a}$$

$$T_{\bar{\nu}}(q) = T_2(u_2) = \int_0^\infty e^{-k_2 u_2} f_2(k_2)\, dk_2. \tag{4.3.18b}$$

Letting $k_2 = k'' q_c/q$ in Eq. (4.3.18b), we then have

$$T_2(u_1) = \int_0^\infty e^{-k'' u_1} f_2^*(k'')\, dk'', \tag{4.3.18c}$$

where the probability distribution function

$$f_2^*(k'') = \frac{q_c}{q} f_2\left(\frac{q_c}{q} k''\right) = L^{-1}(T_2(u_1)). \tag{4.3.19a}$$

From Eq. (4.3.18a), by letting $k_1 = k'$ for convenience of presentation, we also have

$$f_1(k') = L^{-1}(T_1(u_1)). \tag{4.3.19b}$$

It follows that Eq. (4.3.17c) can be rewritten in the form

$$\begin{aligned} T_{\bar{\nu}}(q, q_c) &= \int_0^\infty e^{-k' u_1} f_1(k')\, dk' \cdot \int_0^\infty e^{-k'' u_1} f_2^*(k'')\, dk'' \\ &= \int_0^\infty \int_0^\infty e^{-(k'+k'')u_1} f_1(k') f_2^*(k'')\, dk'\, dk''. \end{aligned} \tag{4.3.20a}$$

We may define $k = k' + k''$. By replacing k' with $k - k''$, interchanging the double integrals and their limits, and employing the convolution theorem of the Laplace

transform given by

$$f(k) = L^{-1}(T_{\bar{\nu}}(q, q_c)) = \int_0^k f_1(k - k'') f_2^*(k'')\, dk'', \tag{4.3.20b}$$

we can prove that

$$T_{\bar{\nu}}(q, q_c) = \int_0^\infty e^{-ku_1} f(k)\, dk = \int_0^1 e^{-k(g)u_1}\, dg. \tag{4.3.20c}$$

Because the mixing ratio for carbon dioxide q_c is constant, we may apply the correlated condition for an inhomogeneous path to Eq. (4.3.20c) to obtain

$$T_{\bar{\nu}}(q, q_c) \cong \int_0^1 \exp\left[-q_c \int k(g, T, p, q)\rho\, dz\right] dg, \tag{4.3.21a}$$

where the cumulative probability function is given by

$$g(k, p, T, q) = \int_0^k f(k, p, T, q)\, dk. \tag{4.3.21b}$$

The CKD for a single-mixture gas requires the same correlated assumptions as those for an individual gas, except that an additional variable, q, is needed. To facilitate the computation of $k(g, p, T, q)$, efficient parameterization can be developed for a number of pressure, temperature, and H_2O mixing ratios.

4.4 Band Models

Band models are traditional approaches that simplify the computation of the spectral transmittance. The atmosphere is assumed to be homogeneous so that analytical expressions may be developed. We first define spectral absorptance in the form

$$A_{\bar{\nu}}(u) = 1 - T_{\bar{\nu}} = \frac{1}{\Delta\nu} \int_{\Delta\nu} (1 - e^{-k_\nu u})\, d\nu. \tag{4.4.1}$$

The quantity $A_{\bar{\nu}}\Delta\nu$ is referred to as the equivalent width $W(u)$. It is the width of an infinitely strong line of rectangular shape, which would be the same as the actual absorption of a single line (Fig. 4.9). The concept of equivalent width plays an important role in the development of band models.

4.4.1 A Single Line

Using a single Lorentz line, introducing two new variables, $x = Su/2\pi\alpha$ and $\tan y/2 = (\nu - \nu_0)/\alpha$, and extending the wavenumber integration from $-\infty$ to ∞, the spectral absorptance can be shown to be

$$A_{\bar{\nu}} = \frac{\alpha}{\Delta\nu} \int_{-\pi}^{\pi} \{1 - \exp[-x(1 + \cos y)]\}\, d(\tan y/2). \tag{4.4.2}$$

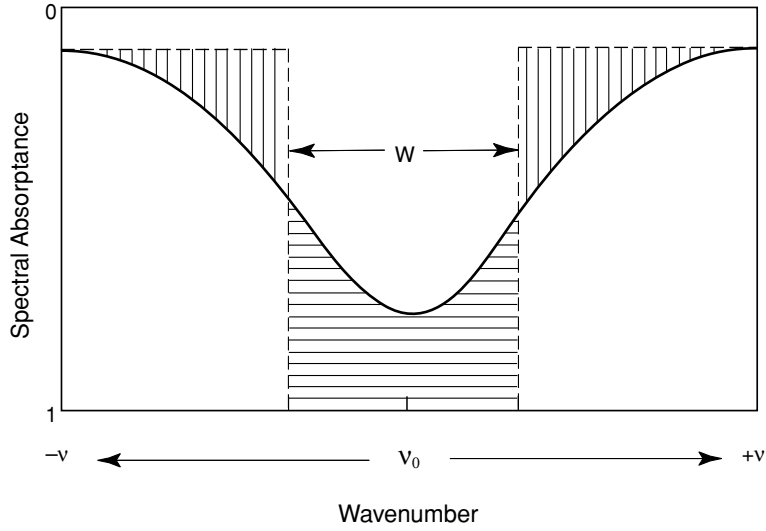

Figure 4.9 The definition of equivalent width, $W = A_{\bar{\nu}}\Delta\bar{\nu}$, where $A_{\bar{\nu}}$ represents the spectral absorptance for a spectral interval $\Delta\nu$. It is the width of an infinitely strong line of rectangular shape that is the same as the absorption of a single line.

Performing integration by parts and carrying out further trigonometric manipulations yield

$$A_{\bar{\nu}} = \frac{\alpha x e^{-x}}{\Delta\nu} \int_{-\pi}^{\pi} (e^{-x\cos y} - \cos y e^{-x\cos y})\, dy. \tag{4.4.3}$$

The integral representation of the Bessel function is given by

$$J_n(x) = \frac{i^{-n}}{\pi} \int_0^{\pi} e^{ix\cos\theta} \cos n\theta\, d\theta, \tag{4.4.4a}$$

and the modified Bessel function of the first kind of order n is

$$I_n(x) = i^{-n} J_n(ix), \tag{4.4.4b}$$

where $i = \sqrt{-1}$. Thus, in terms of the modified Bessel function, equivalent width is given by

$$W = A_{\bar{\nu}}\Delta\nu = 2\pi\alpha L(x) = 2\pi\alpha x e^{-x}[I_0(x) + I_1(x)], \tag{4.4.5}$$

where $L(x)$ is known as the Ladenburg and Reiche function.

In the case of weak-line absorption, either k_ν or u is small, so that $k_\nu u \ll 1$. Spectral absorptance is approximately given by

$$A_{\bar{\nu}} \cong \frac{1}{\Delta\nu} \int_{-\infty}^{\infty} k_\nu u\, d\nu = \frac{Su}{\Delta\nu}, \tag{4.4.6}$$

based on the definition of line intensity, regardless of the line shape. Absorptance,

under the limits of weak-line approximations, is directly proportional to the path length and is called the region of *linear absorption*. On the other hand, if $Su/\pi\alpha \gg 1$, absorptance approaches 1 in the line center region. We may omit the half-width α in the denominator of the Lorentz profile so that

$$A_{\bar{\nu}}(u) = \frac{1}{\Delta\nu}\int_{-\infty}^{\infty}\left[1 - \exp\left(\frac{-S\alpha u}{\pi(\nu-\nu_0)^2}\right)\right]d\nu. \tag{4.4.7a}$$

Using the known integration formula (Exercise 3.6), we find

$$A_{\bar{\nu}}(u) = 2\sqrt{S\alpha u}/\Delta\nu. \tag{4.4.7b}$$

Absorptance is, therefore, proportional to the square root of the path length and is in the region of the so-called *square root absorption*. Approximations for the weak- and strong-line limits can also be derived directly from Eq. (4.4.5) (Exercise 4.2). Summarizing the preceding discussion, the equivalent width for a spectral line can be written as follows:

$$W = A_{\bar{\nu}}(u)\Delta\nu = \begin{cases} Su, & \text{weak-line,} \\ 2\sqrt{S\alpha u}, & \text{strong-line.} \end{cases} \tag{4.4.8}$$

These two limits are useful in the development of approximations for use in infrared radiative transfer calculations.

4.4.2 Regular Band Model

Inspection of the Q-branch of the 15 μm CO_2 band indicates that a single line may repeat itself periodically (or regularly) as shown in Fig. 4.6b. This configuration led Elsasser (1938) to the development of the regular band model. In this case, the absorption coefficient at a wavenumber displacement ν from the center of one particular line is then

$$k_\nu = \sum_{i=-\infty}^{\infty}\frac{S\alpha/\pi}{(\nu - i\delta)^2 + \alpha^2}, \tag{4.4.9}$$

where δ is the line spacing. From the Mittag–Leffler theorem (Whittaker and Watson, 1940), we can prove that this infinite sum can be expressed in terms of periodic and hyperbolic functions as follows:

$$k_\nu = \frac{S}{\delta}\frac{\sinh\beta}{\cosh\beta - \cos\gamma}, \tag{4.4.10}$$

where $\beta = 2\pi\alpha/\delta$ and $\gamma = 2\pi\nu/\delta$. By transforming the variables, the spectral transmittance may be expressed by

$$T_{\bar{\nu}}(u) = \frac{1}{\delta}\int_{-\delta/2}^{\delta/2} e^{-k_\nu u}d\nu = \frac{1}{2\pi}\int_{-\pi}^{\pi} e^{-k_\nu(\gamma)u}d\gamma. \tag{4.4.11a}$$

The differential value is

$$\frac{dT_{\bar{\nu}}(u)}{du} = -\frac{1}{2\pi}\int_{-\pi}^{\pi} e^{-k_\nu u} k_\nu d\gamma. \tag{4.4.11b}$$

To derive an analytical expression, we define

$$\cos\rho = \frac{1-\cosh\beta\cos\gamma}{\cosh\beta-\cos\gamma}. \tag{4.4.12a}$$

It follows from Eq. (4.4.10) that

$$d\rho = -\frac{\sinh\beta}{\cosh\beta-\cos\gamma}d\gamma = -k_\nu\frac{\delta}{S}\,d\gamma. \tag{4.4.12b}$$

Substituting Eqs. (4.4.10) and (4.4.12b) into Eq. (4.4.11b) leads to

$$\frac{dT_{\bar{\nu}}}{du} = -\frac{S}{2\pi\delta}\int_{-\pi}^{\pi}\exp\left(-\frac{Su}{\delta}\frac{\cosh\beta-\cos\rho}{\sinh\beta}\right)d\rho. \tag{4.4.13a}$$

We then define a new variable $y = Su/(\delta\sinh\beta)$ to obtain

$$\begin{aligned}\frac{dT_{\bar{\nu}}}{dy} &= -\frac{\sinh\beta}{2\pi}\int_{-\pi}^{\pi}\exp(-y\cosh\beta - y\cos\rho)\,d\rho \\ &= -\sinh\beta e^{-y\cosh\beta}J_0(iy).\end{aligned} \tag{4.4.13b}$$

Since $T_{\bar{\nu}} = 0$ when u (or y) $\to\infty$, we have

$$\begin{aligned}T_{\bar{\nu}} &= \int_0^{T_{\bar{\nu}}} dT_{\bar{\nu}} = \sinh\beta\int_y^\infty e^{-y\cosh\beta}J_0(iy)\,dy \\ &= \int_z^\infty e^{-z\coth\beta}J_0(iz/\sinh\beta)\,dz,\end{aligned} \tag{4.4.14}$$

where $z = y\sinh\beta$. This is the Elsasser transmittance that can be evaluated numerically. Further approximations and simplifications also can be made to this model. Since $\alpha \ll \delta$ and $\beta \to 0$, we find

$$\coth\beta \approx \frac{1}{\beta}+\frac{\beta}{3}, \quad \operatorname{csch}\beta \approx \frac{1}{\beta}-\frac{\beta}{6}, \tag{4.4.15a}$$

and

$$\begin{aligned}J_0(iz\operatorname{csch}\beta) &\approx e^{z\operatorname{csch}\beta}\Big/\sqrt{2\pi z\operatorname{csch}\beta} \\ &\approx \exp\left[z\left(\frac{1}{\beta}-\frac{\beta}{6}\right)\right]\Big/\sqrt{2\pi z/\beta}.\end{aligned} \tag{4.4.15b}$$

With these approximations, Eq. (4.4.14) becomes

$$T_{\bar{\nu}} = \frac{1}{\sqrt{2\pi}}\int_z^\infty\sqrt{\beta/z}\,e^{-z\beta/2}dz. \tag{4.4.16}$$

Finally, we set $x^2 = z\beta/2$; the absorptance can now be expressed by

$$A_{\bar{\nu}} = 1 - \frac{2}{\sqrt{\pi}} \int_x^\infty e^{-x^2} dx. \tag{4.4.17a}$$

By noting that $(2/\sqrt{\pi}) \int_0^\infty e^{-x^2} dx = 1$, we have

$$A_{\bar{\nu}} = \frac{2}{\sqrt{\pi}} \int_0^x e^{-x^2} dx = \operatorname{erf}(x) = \operatorname{erf}\left(\frac{\sqrt{\pi S \alpha u}}{\delta} \right). \tag{4.4.17b}$$

Values of $\operatorname{erf}(x)$ can be obtained from standard mathematical tables. This is referred to as the Elsasser model. For small values of x, $A_{\bar{\nu}} = 2x/\sqrt{\pi} = 2\sqrt{S\alpha u}/\delta$. This is the region of square root absorption denoted in Eq. (4.4.7b).

4.4.3 Statistical Band Model

On inspection of the water vapor rotational band, the only common feature over a 25 cm^{-1} range is the apparent random line positions (Goody, 1952, 1964). Hence, the absorption of a band with certain random properties should be considered. Let $\Delta\nu$ be a spectral interval consisting of n lines of mean distance δ, so that $\Delta\nu = n\delta$. Let $p(S_i)$ be the probability that the ith line has an intensity S_i, and let p be normalized such that

$$\int_0^\infty p(S_i)\, dS_i = 1, \quad i = 1, \ldots, n. \tag{4.4.18}$$

We may assume that any line has an equal probability of being anywhere in the interval $\Delta\nu$. The mean transmittance is found by averaging the transmittance over all line positions and intensities. Hence,

$$\begin{aligned} T_{\bar{\nu}} = {} & \frac{1}{(\Delta\nu)^n} \int_{\Delta\nu} d\nu_1 \cdots \int_{\Delta\nu} d\nu_n \\ & \times \int_0^\infty p(S_1) e^{-k_1 u}\, dS_1 \cdots \int_0^\infty p(S_n) e^{-k_n u}\, dS_n, \end{aligned} \tag{4.4.19a}$$

where k_n denotes the absorption coefficient for the nth line. Since all the integrals are alike, we have

$$\begin{aligned} T_{\bar{\nu}} &= \left[\frac{1}{\Delta\nu} \int d\nu \int_0^\infty p(S) e^{-ku}\, dS \right]^n \\ &= \left[1 - \frac{1}{\Delta\nu} \int d\nu \int_0^\infty p(S)(1 - e^{-ku})\, dS \right]^n. \end{aligned} \tag{4.4.19b}$$

The average equivalent width for n absorption lines may be defined by

$$\bar{W} = \int_0^\infty p(S) \int_{\Delta\nu} (1 - e^{-ku})\, d\nu\, dS. \tag{4.4.20}$$

Noting that $\Delta\nu = n\delta$, the spectral transmittance may then be written in terms of the averaged equivalent width in the form

$$T_{\bar{\nu}}(u) = \left[1 - \frac{1}{n}\left(\frac{\bar{W}}{\delta}\right)\right]^n. \tag{4.4.21a}$$

Since $\lim_{n\to\infty}(1 - x/n)^n \to e^{-x}$, we have

$$T_{\bar{\nu}}(u) = e^{-\bar{W}/\delta}. \tag{4.4.21b}$$

Let the lines be of different intensities, and consider a Poisson distribution for the probability of their intensities in the form

$$p(S) = \frac{1}{\bar{S}} e^{-S/\bar{S}}, \qquad \bar{S} = \int_0^\infty S p(S)\, dS, \tag{4.4.22}$$

where $\bar{S}$ is defined as the mean line intensity. We note that $p(S)$ is normalized to 1, as is required. Inserting this probability function into Eq. (4.4.20) for the average equivalent width, and writing $k_\nu = Sf_\nu$ with f_ν the line-shape factor, we find

$$\bar{W} = \int_{\Delta\nu} \frac{\bar{S} f_\nu u}{1 + \bar{S} f_\nu u}\, d\nu. \tag{4.4.23}$$

Using the Lorentz line shape for f_ν and performing the wavenumber integration in the domain $(-\infty, \infty)$, without introducing significant errors for the integral confined in the $\Delta\nu$ interval, the spectral transmittance for randomly distributed Lorentz lines is given by

$$T_{\bar{\nu}}(u) = \exp\left[-\frac{\bar{S}}{\delta} u \left(1 + \frac{\bar{S}}{\alpha\pi} u\right)^{-1/2}\right]. \tag{4.4.24}$$

Thus the spectral transmittance for the random model can be expressed as a function of two parameters, $\bar{S}/\delta$ and $\bar{S}/\alpha\pi$, apart from the path length u. This is referred to as the *Goody random model*. For a given spectral interval $\Delta\nu$, these two parameters may be derived by fitting the random model with line-by-line data. For the computation of fluxes in the atmosphere, the device of the spectral interval must ensure that the Planck flux does not vary significantly.

On the basis of the preceding discussion, the average equivalent width for the random model is

$$\bar{W} = \bar{S} u \left(1 + \frac{\bar{S} u}{\alpha\pi}\right)^{-1/2}. \tag{4.4.25a}$$

The average equivalent width for n individual lines with equivalent widths of W_i is simply

$$\bar{W} = \sum_{j=1}^{n} \frac{W_j}{n}. \tag{4.4.25b}$$

The spectral transmittance given in Eq. (4.4.24) is general and should be valid under the limits of weak- and strong-line approximations. Thus, for weak-line approximations where $\bar{S}u/\alpha\pi \ll 1$, we have

$$\frac{\bar{W}}{\delta} \approx \frac{\bar{S}}{\delta}u. \tag{4.4.26}$$

However, by using the equivalent width for a spectral line denoted by the subscript j under the limits of weak-line approximations, we have

$$\bar{W} = \frac{1}{n}\sum_{j=1}^{n} W_j(\text{weak}) \approx \frac{1}{n}\sum_{j=1}^{n} S_j u. \tag{4.4.27}$$

From Eqs. (4.4.26) and (4.4.27), we obtain

$$\frac{\bar{S}}{\delta} = \sum_{j=1}^{n} \frac{S_j}{\Delta\nu} = a_{\bar{\nu}}, \tag{4.4.28}$$

where $a_{\bar{\nu}}$ is so defined. Following the same procedure under the limits of strong-line approximations, we find

$$\frac{\sqrt{\pi\alpha\bar{S}}}{\delta} = 2\sum_{j=1}^{n} \frac{\sqrt{S_j\alpha_j}}{\Delta\nu} = b^*_{\bar{\nu}}. \tag{4.4.29}$$

If we define $b_{\bar{\nu}} = \pi\alpha/\delta$, then $b^*_{\bar{\nu}} = \sqrt{a_{\bar{\nu}}b_{\bar{\nu}}}$. It follows that

$$b_{\bar{\nu}} = \left(2\sum_{j=1}^{n}\sqrt{S_j\alpha_j}\right)^2 \Bigg/ \left(\Delta\nu\sum_{j=1}^{n} S_j\right). \tag{4.4.30}$$

Thus, the spectral transmittance may be written in the form

$$T_{\bar{\nu}}(u) = \exp[-a_{\bar{\nu}}u(1 + ua_{\bar{\nu}}/b_{\bar{\nu}})^{-1/2}]. \tag{4.4.31}$$

The band parameters $a_{\bar{\nu}}$ and $b_{\bar{\nu}}$ are functions of two variables: $\sum_j S_j$ and $\sum_j \sqrt{S_j\alpha_j}$. These variables can be computed from line-by-line data.

The spectral transmittance for the random model depends on two parameters, $a_{\bar{\nu}}$ and $a_{\bar{\nu}}/b_{\bar{\nu}}$. Examination of these parameters reveals that a further simplification may be obtained by defining a parameter referred to as the *generalized absorption coefficient,* $\ell_{\bar{\nu}}$, such that $a_{\bar{\nu}} = a\ell_{\bar{\nu}}$ and $a_{\bar{\nu}}/b_{\bar{\nu}} = b\ell_{\bar{\nu}}$, where the coefficients a and b are certain constants. Thus, a one-parameter representation of the spectral transmittance for the random model may be expressed by

$$T_{\bar{\nu}}(u) = \exp[-a\ell_{\bar{\nu}}u(1 + b\ell_{\bar{\nu}}u)^{-1/2}]. \tag{4.4.32}$$

The generalized absorption coefficient was originally developed by Elsasser (1942). Under the limits of strong- and weak-line approximations, we have

$$T_{\bar{\nu}}(u) \cong \begin{cases} \exp(-a\ell_{\bar{\nu}}u), & \text{weak-line,} \\ \exp(-c\ell^*_{\bar{\nu}}u^*), & \text{strong-line,} \end{cases} \tag{4.4.33}$$

where $c = a/\sqrt{b}$, $\ell_{\bar{\nu}}^* = \sqrt{\ell_{\bar{\nu}}}$, and $u^* = \sqrt{u}$. The transmittance is now expressed by a simple exponential function in terms of the generalized absorption coefficient, which can be obtained from the band parameters using statistical fitting procedures.

The random model just described utilizes the probability distribution function given in Eq. (4.4.22). In many cases, it has been found that this exponential intensity distribution substantially underestimates the number of low-intensity lines (Malkmus, 1967). The line intensity is governed by the Boltzmann factor in the form $S \sim \exp(-hcE/KT)$, where E is the lower energy level. Thus, dE/dS is proportional to S^{-1}. The probability distribution function $p(S)$ must be proportional to dn/dS, where n is the number density of energy levels. However, dn/dE is approximately constant since, in many cases, the energy levels are approximately equally spaced. It follows that $p(S) \sim (dE/dS)(dn/dE) \sim dE/dS \sim S^{-1}$. Thus, the S^{-1} dependence remains a dominating influence on the probability distribution function. For this reason, it is necessary to use a normalized probability distribution function for line intensity in the form

$$p(S) \sim \frac{1}{S} e^{-s/\bar{s}}. \tag{4.4.34a}$$

Using the normalized form of the probability distribution function, we can derive, after lengthy mathematical manipulations, the following spectral transmittance:

$$T_{\bar{\nu}}(u) = \exp\left\{ - c_{\bar{\nu}} \left[(1 + d_{\bar{\nu}} u)^{1/2} - 1 \right] \right\}, \tag{4.4.34b}$$

where the two parameters are defined by the line data as follows:

$$c_{\bar{\nu}} = 2 \left(\sum_j \sqrt{\alpha_j S_j} \right)^2 \Bigg/ \left(\Delta\nu \sum_j S_j \right),$$

$$d_{\bar{\nu}} = \left(\sum_j S_j \right)^2 \Bigg/ \left(\sum_j \sqrt{\alpha_j S_j} \right)^2. \tag{4.4.34c}$$

This is referred to as the *Malkmus random model*. In terms of line parameters, we can prove that $c_{\bar{\nu}} = \pi\alpha/2\delta$, and $d_{\bar{\nu}} = 4\bar{S}/\pi\alpha$ (Exercise 4.8).

4.4.4 Application to Nonhomogeneous Atmospheres

In band models, it is assumed that the absorption coefficient is independent of temperature and pressure. To incorporate these effects in the calculation of spectral transmittance, we should first define the optical depth by

$$\tau = \int_u k_\nu(p, T)\, du. \tag{4.4.35}$$

The primary objective of approximate solutions for nonhomogeneous path lengths is to transform the transfer problem to that of a homogeneous path defined by a reference pressure, p_r, and a reference temperature, T_r, so that analytical exponential

functions can be employed for spectral transmittance calculations. In the limit of strong-line approximations denoted in Eq. (4.3.9), the wavenumber-dependent term can be factored out. Moreover, the half-width can be written as

$$\alpha(p, T) = \alpha(p_r, T_r)\left(\frac{p}{p_r}\right)\left(\frac{T_r}{T}\right)^n. \tag{4.4.36}$$

Thus, to a good approximation, we can prove that

$$k_\nu(p, T) \cong k_\nu(p_r, T_r)\left(\frac{p}{p_r}\right)\left(\frac{T_r}{T}\right)^n, \tag{4.4.37a}$$

where we have set

$$\sum_j \frac{S_j(T)\alpha_j(p_r, T_r)}{(\nu - \nu_{0j})^2} \Bigg/ \sum_j \frac{S_j(T_r)\alpha_j(p_r, T_r)}{(\nu - \nu_{0j})^2} \approx 1. \tag{4.4.37b}$$

The case in which the wavenumber, pressure, and temperature are decoupled is referred to as the *one-parameter scaling approximation*. It is particularly useful for application to the rotational band of water vapor (Chou and Arking, 1980).

From Eq. (4.4.37a), we may define a scaled path length such that

$$\tau = k_\nu(p_r, T_r)\tilde{u}, \tag{4.4.38a}$$

where

$$\tilde{u} = \int_u \left(\frac{p}{p_r}\right)\left(\frac{T_r}{T}\right)^n du. \tag{4.4.38b}$$

It follows that by replacing u with $\tilde{u}$, the spectral transmittance may be evaluated by using the absorption coefficient at a reference temperature and pressure. The scaling approximation for flux and cooling-rate calculations using $n = 1/2$ was originally proposed by Elsasser and Culbertson (1960).

Further, we may also search for an adjusted absorption coefficient such that

$$\tau = \int_u k_\nu(p, T)\, du = k_\nu(\tilde{p}, \tilde{T})u. \tag{4.4.39a}$$

Using the Lorentz line profile, we have

$$k_\nu(\tilde{p}, \tilde{T}) = \sum_j \tilde{S}_j \tilde{f}_{\nu j} = \sum_j \frac{\tilde{S}_j}{\pi} \frac{\tilde{\alpha}_j}{(\nu - \nu_{0j})^2 + \tilde{\alpha}_j^2}. \tag{4.4.39b}$$

Two adjusted parameters, $\tilde{S}$ and $\tilde{\alpha}$, are required to satisfy Eq. (4.4.39a). This is referred to as the *two-parameter approximation*.

In reference to Eq. (4.4.1), the average equivalent width of a nonhomogeneous path is

$$\bar{W} = A_{\bar{\nu}}(u)\Delta\nu = \int_{\Delta\nu} \left[1 - \exp\left(-\int_u \sum_j S_j f_{\nu j}\, du\right)\right] d\nu. \tag{4.4.40a}$$

In the weak-line limit, we have

$$\bar{W} \cong \int_{\Delta\nu} \int_u \sum_j S_j f_{\nu j}\, du\, d\nu = \int_u \sum_j S_j\, du, \tag{4.4.40b}$$

regardless of the line shape. Moreover, using the Lorentz profile, the average equivalent width given in Eq. (4.4.40a) may be written in the form

$$\bar{W} = \int_{\Delta\nu} \left[1 - \exp\left(- \int_u \sum_j \frac{S_j}{\pi} \frac{\alpha_j}{(\nu - \nu_{0j})^2 + \alpha_j^2}\, du \right) \right] d\nu. \tag{4.4.40c}$$

In the strong-line limit, absorption near the line-center region is nearly saturated. The average equivalent width in this case is not very sensitive to the absorption coefficient. Hence, we may select any half-width, say α', to replace α in the denominator of Eq. (4.4.40c). To find the α' that also satisfies the weak-line limit, we must have

$$\bar{W} \cong \int_{\Delta\nu} \int_u \sum_j \frac{S_j}{\pi} \frac{\alpha_j}{(\nu - \nu_{0j})^2 + \tilde{\alpha}_j^2}\, du\, d\nu \cong \int_u \sum_j \frac{\alpha_j}{\tilde{\alpha}_j} S_j\, du, \tag{4.4.40d}$$

where $\Delta\nu$ is set from $-\infty$ to ∞ for mathematical convenience, and $\tilde{\alpha}$ is the specific α' that fulfills the requirements of both the strong- and weak-line limits. Since $\alpha_j/\tilde{\alpha}_j \cong p/\tilde{p}$, combining Eqs. (4.4.40d) and (4.4.40b) gives

$$\tilde{p} = \int_u p\bar{S}\, du \Big/ \int_u \bar{S}\, du, \tag{4.4.41}$$

where $\bar{S}$ is the mean line intensity. The effect of pressure on absorption is evident through the line half-width. The preceding scaling serves to adjust the pressure variation along the path.

Furthermore, from the equivalent width given in Eqs. (4.4.40a) and (4.4.40b), we may select an adjusted $\tilde{S}_j$ such that

$$\int_u \sum_j S_j\, du = u \sum_j \tilde{S}_j. \tag{4.4.42}$$

This defines the scaled mean line intensity, regardless of the line shape, in the form

$$\tilde{\bar{S}} = \int \bar{S}\, du/u. \tag{4.4.43a}$$

The effect of temperature on absorption is exerted through its dependence on the line strength. This part of scaling is to account for the nonisothermal path. Alternatively, we may select a reference $\bar{S}$, say $\bar{S}_r$, and adjust the path length u such that

$$\tilde{u} = \int_u \frac{\bar{S}}{\bar{S}_r}\, du. \tag{4.4.43b}$$

Equations (4.4.41) and (4.4.43) constitute the so-called *Curtis–Godson* (CG) *approximation* for nonhomogeneous atmospheres, independently proposed by Curtis (1952)

and Godson (1953). Its validity has been checked by Walshaw and Rodgers (1963), who performed extensive cooling-rate calculations using a line-by-line integration program. Errors introduced by the CG approximation are less than a few percent for the H_2O rotational and 15 μm CO_2 bands. The CG approximation, however, is less satisfactory for the 9.6 μm O_3 band.

van de Hulst (1945) innovated a more general technique for application to a nonhomogeneous atmosphere and demonstrated that the Voigt profile can be readily incorporated in this technique. Consider the cosine transformation of the optical depth in the form

$$\tilde{g}(t) = \int_{-\infty}^{\infty} \tau(\nu) \cos \nu t \, d\nu = \int_u g(t) \, du, \tag{4.4.44a}$$

where

$$\tau(\nu) = \frac{1}{\pi} \int_0^{\infty} \tilde{g}(t) \cos \nu t \, dt, \tag{4.4.44b}$$

$$g(t) = \int_{-\infty}^{\infty} k_\nu \cos \nu t \, d\nu. \tag{4.4.44c}$$

On substituting the expressions of the absorption coefficient for Lorentz, Doppler, and Voigt line shapes, we find

$$g(t) = \begin{cases} S \exp(-\alpha t), & \text{Lorentz} \\ S \exp(-\alpha_D^2 t^2/4), & \text{Doppler} \\ S \exp[-(\alpha t + \alpha_D^2 t^2/4)], & \text{Voigt.} \end{cases} \tag{4.4.45}$$

By using the Voigt profile and defining the scaled path length $\tilde{u}$ and the scaled line widths, $\tilde{\alpha}$ and $\tilde{\alpha}_D$, we obtain

$$\tilde{g}(t) = \int_u S \exp\left[-\left(\alpha t + \frac{\alpha_D^2 t^2}{4}\right)\right] du \equiv S_r \tilde{u} \exp\left[-\left(\frac{\tilde{\alpha} t + \tilde{\alpha}_D^2 t^2}{4}\right)\right]. \tag{4.4.46}$$

If we take the first two terms in the expansion and match t^n in the expansion for $n = 0$ and 1, we have

$$\tilde{u} = \int_u \left(\frac{S}{S_r}\right) du, \tag{4.4.47a}$$

$$\tilde{\alpha} = \frac{1}{\tilde{u}} \int_u \alpha \left(\frac{S}{S_r}\right) du. \tag{4.4.47b}$$

The Doppler width, α_D, is a function of temperature only. Thus, if the temperature does not vary significantly along the nonhomogeneous path, we may set $\tilde{\alpha}_D = \alpha_D$. Equations (4.4.47a) and (4.4.47b) are equivalent to the Curtis–Godson relations.

4.5 Broadband Approaches to Flux Computations

4.5.1 Broadband Emissivity

The essence of the broadband emissivity approach for the calculation of infrared fluxes and heating rates is to use temperature directly in terms of the Stefan–Boltzmann law instead of the Planck function. The early development of broadband emissivity methods was based on the concept of the radiation chart from which the flux integration may be carried out by using graphs and tables (Elsasser, 1942; Möller, 1943; Yamamoto, 1952).

Based on Eq. (4.2.10), the total upward and downward fluxes in the u coordinate may be written

$$F^{\uparrow}(u) = \int_0^{\infty} \pi B_{\nu}(T_s) T_{\nu}^{f}(u) d\nu + \int_0^{\infty} \int_0^{u} \pi B_{\nu}(u') \frac{dT_{\nu}^{f}(u-u')}{du'} du'\, d\nu, \quad (4.5.1a)$$

$$F^{\downarrow}(u) = \int_0^{\infty} \int_{u_1}^{u} \pi B_{\nu}(u') \frac{dT_{\nu}^{f}(u'-u)}{du'} du'\, d\nu. \quad (4.5.1b)$$

In order to express the upward and downward fluxes in terms of broadband emissivity, we may define isothermal broadband flux emissivity in the form

$$\epsilon^{f}(u, T) = \int_0^{\infty} \pi B_{\nu}(T)\left[1 - T_{\nu}^{f}(u)\right] \frac{d\nu}{\sigma T^4}. \quad (4.5.2)$$

Consider a plane-parallel atmosphere divided into a number of layers such that each of them may be thought of as an isothermal layer. We may then write

$$F^{\uparrow}(u) \cong \sigma T_s^4 [1 - \epsilon^{f}(u, T_s)] - \int_0^{u} \sigma T^4(u') \frac{d\epsilon^{f}(u-u', T(u'))}{du'} du', \quad (4.5.3a)$$

$$F^{\downarrow}(u) \cong \int_u^{u_1} \sigma T^4(u') \frac{d\epsilon^{f}(u'-u, T(u'))}{du'} du'. \quad (4.5.3b)$$

Computations of fluxes and cooling rates that use the broadband emissivity definition in Eqs. (4.5.3a,b) have been performed by numerous researchers.

In numerical calculations, Eq. (4.5.2) for broadband flux emissivity is expressed in terms of a finite sum over spectral bands, $\Delta\nu_i$, for three principal absorbers: CO_2, H_2O and O_3. Let $u_1(= u_w)$, $u_2(= u_c)$, and $u_3(= u_0)$ denote the path lengths for H_2O, CO_2 and O_3, respectively. Then we may write

$$\epsilon^{f}(u_j, T) = \sum_i \pi B_{\bar{\nu},i}(T)\left[1 - T_{\bar{\nu},i}^{f}(u_j)\right] \frac{\Delta\nu_i}{\sigma T^4}, \quad j = 1, 2, 3. \quad (4.5.4)$$

As a good approximation, we may replace the diffuse spectral transmittance by the spectral transmittance, $T_{\bar{\nu}}(u/\bar{\mu})$, using the diffusivity factor $1/\bar{\mu} = 1.66$. The spectral transmittance can be generated from data via detailed line-by-line computations or band models for a homogeneous path. Figure 4.10 shows the broadband flux emissivities for water vapor and carbon dioxide as functions of the path length for a number

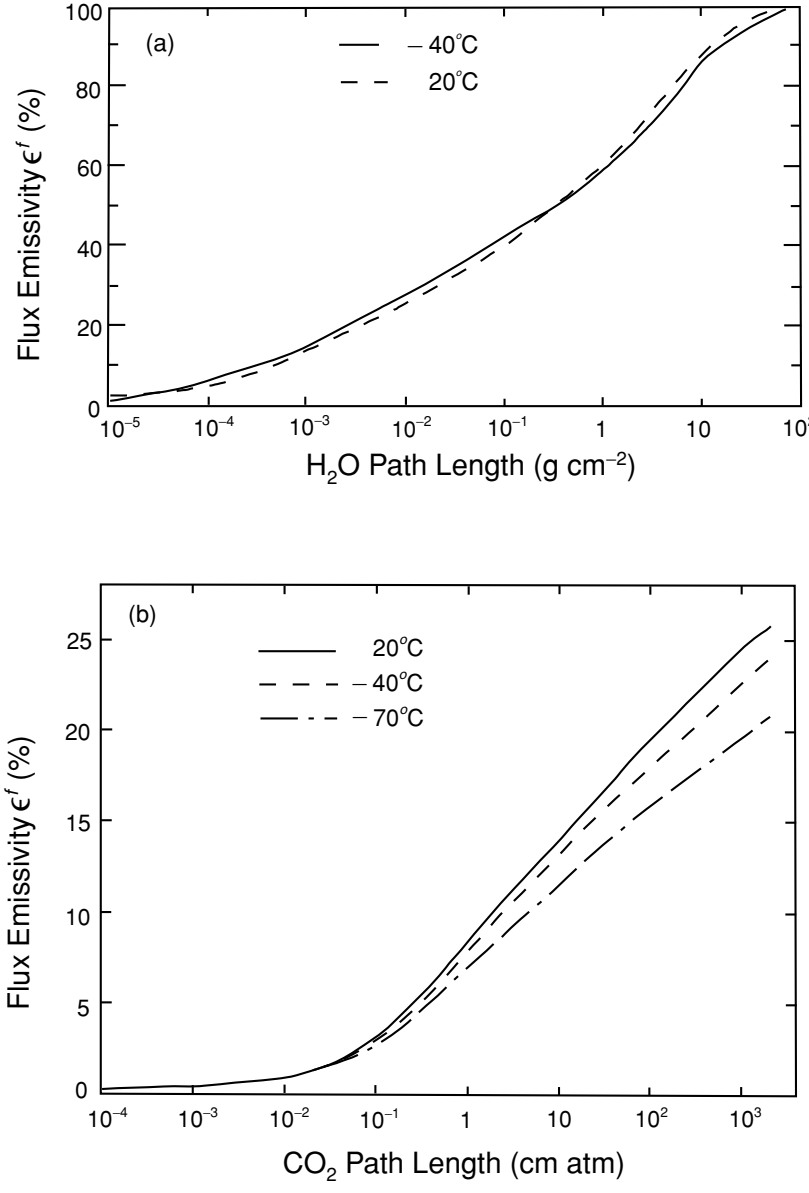

Figure 4.10 Broadband flux emissivity for (a) water vapor and (b) carbon dioxide covering the entire thermal infrared spectrum as a function of path length and temperature. Note that 1 g $cm^{-2} = 2.24 \times 10^4/M$ cm atm, where M is the molecular weight of an individual gas.

of temperatures. For water vapor, the effect of temperature on emissivity is relatively small. For carbon dioxide, however, the temperature dependence of larger path lengths appears quite pronounced.

The total emission of an isothermal atmosphere is the sum of individual emissions due to various gases. However, the overlap of the H_2O rotational and 15 μm CO_2 absorption lines is significant. Thus, it is necessary to make a proper correction to circumvent the overestimation of H_2O and CO_2 emissions. The emissivity for the overlap region can be expressed exactly by

$$\epsilon^f(u_w, u_c, T) = \int_0^\infty \pi B_\nu(T)[1 - T_\nu(\bar{u}_w, \bar{u}_c)]\frac{d\nu}{\sigma T^4}, \tag{4.5.5}$$

where $\bar{u}_w = u_w/\bar{\mu}$ and $\bar{u}_c = u_c/\bar{\mu}$. From the definition of monochromatic transmittance, its value for two absorbing gases is the product of the individual value for each absorbing gas. It follows that

$$T_\nu(\bar{u}_w, \bar{u}_c) = T_\nu(\bar{u}_w)T_\nu(\bar{u}_c). \tag{4.5.6}$$

With this relation, which is valid only for monochromatic radiation, we may express the emissivity of the overlap region in terms of the individual emissivities in the form

$$\epsilon^f(u_w, u_c, T) = \epsilon^f(u_w, T) + \epsilon^f(u_c, T) - \Delta\epsilon^f(u_w, u_c, T), \tag{4.5.7}$$

where the correction term is

$$\begin{aligned}\Delta\epsilon^f(u_w, u_c, T) &= \int_0^\infty \pi B_\nu(T)[1 - T_\nu(\bar{u}_w)][1 - T_\nu(\bar{u}_c)]\frac{d\nu}{\sigma T^4} \\ &\cong \sum_i \pi B_{\bar{\nu},i}(T) \int_{\Delta\nu_i} [1 - T_\nu(\bar{u}_w)[1 - T_\nu(\bar{u}_c)]\frac{d\nu}{\sigma T^4}.\end{aligned} \tag{4.5.8}$$

If the variation in either $T_\nu(\bar{u}_w)$ or $T_\nu(\bar{u}_c)$ is smaller than their products, we may carry out a wavenumber integration over either one to obtain

$$\Delta\epsilon^f(u_w, u_c, T) \cong \sum_i \pi B_{\bar{\nu},i}(T)[1 - T_{\bar{\nu},i}(\bar{u}_w)][1 - T_{\bar{\nu},i}(\bar{u}_c)]\frac{\Delta\nu_i}{\sigma T^4}. \tag{4.5.9}$$

This appears to be a good approximation and has been used to evaluate the H_2O–CO_2 overlap in the context of the broadband emissivity for flux computations. The computation of broadband flux emissivities for H_2O, CO_2, and O_3 has been correctly carried out by Staley and Jurica (1970, 1972) using the generalized absorption coefficients presented by Elsasser and Culbertson (1960). A review of various methods that can be used to construct the broadband emissivity for flux and heating rate calculations has been presented by Chou *et al.* (1991).

4.5.2 Newtonian Cooling Approximation

The general circulation of the middle atmosphere from ~15 to 90 km is driven by differential vertical and horizontal radiative heating. Absorption of solar insolation in

this region is primarily generated by O_3 and O_2. This absorption is largely balanced by radiative cooling throughout much of the stratosphere and parts of the mesosphere produced principally by emission and absorption of thermal IR radiation due to CO_2 and O_3. For middle atmosphere applications, the shape and overlap of absorption lines, the variation in line intensity with temperature, and departures from LTE at high altitudes must be taken into account in the computations.

Many attempts have been made to develop accurate yet efficient methods to compute IR cooling rates in the middle atmosphere in connection with dynamic models. The most important aspect of radiative cooling from the viewpoint of dynamic circulation is its variation with changes in temperature. In the following, we introduce a method that is based on the cooling-to-space approximation widely used by modelers.

Consider the upward and downward fluxes given in Eqs. (4.2.10a) and (4.2.10b) for a spectral interval in which the variation in Planck fluxes can be neglected. In the height coordinate, we may write

$$F_{\bar{\nu}}^{\uparrow}(z) = \pi B_{\bar{\nu}}(0) T_{\bar{\nu}}^{f}(z) + \int_0^z \pi B_{\bar{\nu}}(z') \frac{d}{dz'} T_{\bar{\nu}}^{f}(z - z')\, dz', \tag{4.5.10a}$$

$$F_{\bar{\nu}}^{\downarrow}(z) = \int_{z_\infty}^z \pi B_{\bar{\nu}}(z') \frac{d}{dz'} T_{\bar{\nu}}^{f}(z' - z)\, dz', \tag{4.5.10b}$$

where z_∞ denotes the height at TOA and $z = 0$ denotes the surface. The net flux at a given level is then

$$F_{\bar{\nu}}(z) = F_{\bar{\nu}}^{\uparrow}(z) - F_{\bar{\nu}}^{\downarrow}(z) = \pi B_{\bar{\nu}}(0) T_{\bar{\nu}}^{f}(z) + \int_0^{z_\infty} \pi B_{\bar{\nu}}(z') \frac{d}{dz'} T_{\bar{\nu}}^{f}(|z - z'|)\, dz'. \tag{4.5.11}$$

The cooling rate for a spectral interval is then given by

$$\left(\frac{\partial T}{\partial t}\right)_{\bar{\nu}} = -\frac{1}{\rho C_p} \frac{dF_{\bar{\nu}}(z)}{dz} = -\frac{1}{\rho C_p} \left(\pi B_{\bar{\nu}}(0) \frac{d}{dz} T_{\bar{\nu}}^{f}(z) + \int_0^{z_\infty} \pi B_{\bar{\nu}}(z') \frac{d}{dz'} \frac{d}{dz} T_{\bar{\nu}}^{f}(|z - z'|)\, dz'\right). \tag{4.5.12}$$

Consider an atmosphere with an isothermal temperature profile such that local cooling rates are produced solely from the emission of a local layer. Under this condition we have

$$\left(\frac{\partial T}{\partial t}\right)_{\text{space}} = -\frac{1}{\rho C_p} \pi B_{\bar{\nu}}(z) \frac{d}{dz} T_{\bar{\nu}}^{f}(z_\infty - z). \tag{4.5.13}$$

This is referred to as the *cooling-to-space approximation* in which the cooling rate is dependent on the local temperature but is independent of the temperatures of other levels. Although it is imperfect, this approximation gives reliable results under a number of conditions (Rodgers and Walshaw, 1966). The cooling rate may be expressed in terms of a cooling-to-space term that depends only on the temperature

at that level and a term representing the exchange of radiation between that level and all other levels. This latter term is a function of the entire temperature profile. Thus, we may write

$$Q = \left(\frac{\partial T}{\partial t}\right)_{ir} = \left(\frac{\partial T}{\partial t}\right)_{\text{space}} + \left(\frac{\partial T}{\partial t}\right)_{\text{layer exchange}}. \tag{4.5.14}$$

Based on the preceding consideration, we may construct a simplified method for the calculation of cooling rates in terms of temperature perturbations. Let $T_0(z)$ denote the standard temperature and Q_0 its cooling rate profile. The deviation from this cooling profile is primarily related to temperature variation ΔT, particularly in a CO_2 atmosphere where the CO_2 mixing ratio is constant. Thus, we may write in finite-difference form:

$$\frac{\Delta Q}{\Delta T} = \frac{Q(T_0 + \Delta T) - Q(T_0 - \Delta T)}{2\Delta T} = a_0(z), \tag{4.5.15}$$

where the term a_0 is called the *Newtonian cooling coefficient,* which, when multiplied by ΔT, gives the cooling rate deviation from a standard value Q_0. The preceding discussion provides the foundation for the Newtonian cooling approximation for the calculation of cooling rates in middle atmospheres, where the cooling-to-space approximation is most appropriate. The cooling rate may then be expressed by

$$Q(z) = Q_0(z) + \Delta Q(z) = Q_0(z) + a_0(z)[T(z) - T_0(z)].$$

The Newtonian cooling coefficient can be parameterized from the results computed by a line-by-line program, as illustrated in Dickinson (1973). Shown in Fig. 4.11 are the cooling-rate profiles produced by different types of CO_2, including the fundamental and all the first and second hot bands for $^{12}C^{16}O_2$ and other isotopic bands. It is evident that the hot bands are important contributors to cooling between 50 and 70 km.

4.6 Infrared Radiative Transfer in Cloudy Atmospheres

4.6.1 Fundamentals

In the thermal infrared, scattering, as well as emission and absorption, takes place within clouds. The basic IR radiative transfer equation for gaseous absorption and emission developed previously must, therefore, be modified to account for scattering processes.

Consider a plane-parallel cloud layer, and let the scattering coefficient for cloud particles be β_s and the absorption coefficient for cloud particles plus water vapor within the cloud be β_a. According to Kirchhoff's law, absorption is coupled with emission so that LTE is maintained. The source function in this case is the Planck function, B_ν. Let the source function associated with scattering be J_ν. The radiative

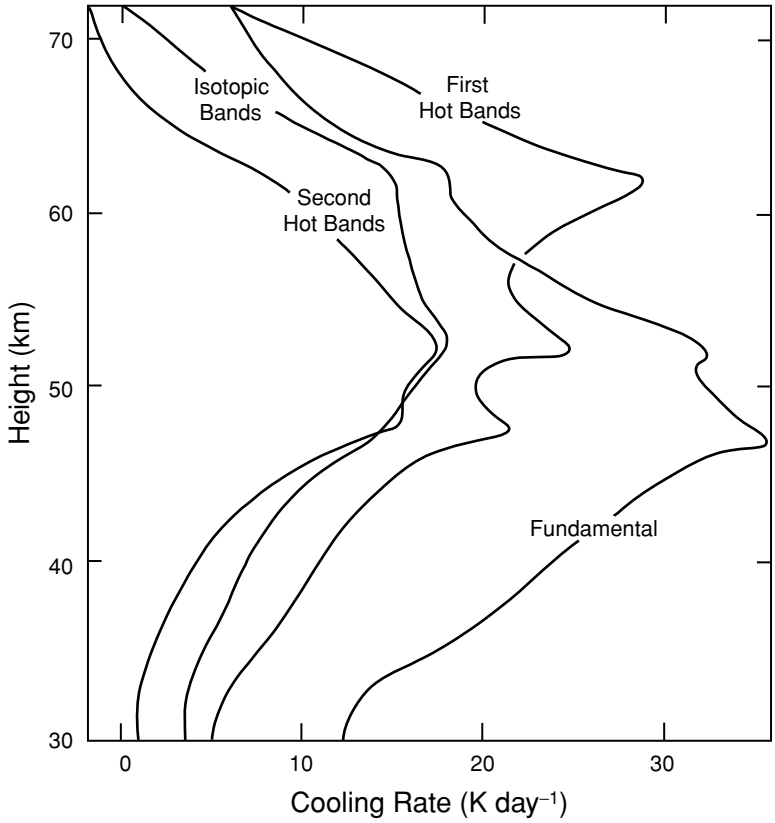

Figure 4.11 Infrared cooling rate given by different types of CO_2 bands for $^{12}C^{16}O_2$, including the fundamental, all the first and second hot bands, and all the fundamental bands of other isotopes (after Dickinson, 1973), based on the line data available at that time.

transfer equation may then be written as

$$\begin{aligned} \mu \frac{dI_\nu}{dz} &= -\beta_a(I_\nu - B_\nu) - \beta_s(I_\nu - J_\nu) \\ &= -\beta_e(I_\nu - S_\nu), \end{aligned} \tag{4.6.1}$$

where the extinction coefficient $\beta_e = \beta_s + \beta_a$, and the source function involving absorption and scattering processes is

$$S_\nu = (\beta_a B_\nu + \beta_s J_\nu)/\beta_e. \tag{4.6.2a}$$

It is an average of the two separate source functions, weighted by their respective absorption and scattering coefficients. The extinction coefficient is the inverse of the mean free path of a photon before scattering or absorption. Using the definition of the single-scattering albedo, $\tilde{\omega}_\nu = \beta_s/\beta_e$, in which a free path will end with a scattering

event, the source function may be expressed by

$$S_\nu = (1 - \tilde{\omega}_\nu) B_\nu + \tilde{\omega}_\nu J_\nu. \tag{4.6.2b}$$

The source function for scattering is associated with multiple scattering processes. In the thermal infrared, it suffices to take the azimuth-independent component:

$$J_\nu = \frac{1}{2} \int_{-1}^{1} P(\mu, \mu') I_\nu(\tau, \mu')\, d\mu', \tag{4.6.3a}$$

where the azimuth-independent phase function is defined by (see Section 3.4.1)

$$P(\mu, \mu') = \frac{1}{2\pi} \int_0^{2\pi} P(\cos\Theta)\, d\phi'. \tag{4.6.3b}$$

If the cloud as a whole is a blackbody, it would behave just like the earth's surface. In this case, radiation from below and above the cloud would not be able to penetrate the cloud. The emitted radiance at the cloud top or bottom is given by the Planck function. Most clouds that are composed of water droplets are black clouds, whereas clouds that are composed of ice crystals are generally non-black.

Shown in Fig. 4.12 is an infrared spectrum covering a spectral region from 9.1 to 17 μm for clear and various cloudy conditions measured from a high-spectral resolution infrared spectrometer aboard a high-flying ER-2 aircraft at about 20 km (see also Fig. 4.3). Strong absorption features are shown by ozone at 9.6 μm (1040 cm^{-1}) and by carbon dioxide at 15 μm (667 cm^{-1}), with weak lines of water vapor scattered in the 10–12 μm (1000–830 cm^{-1}) window of the spectrum. Except for thin cirrus containing small ice particles, clouds composed of water droplets such as low clouds or clouds containing large ice crystals behave like blackbodies or near blackbodies with little variations in the window. Thin cirrus, which are occasionally subvisual, contain small ice crystals with maximum dimensions ranging from about 5 to 20 μm. These clouds have features in the 10 μm window associated with the absorption coefficients of ice crystals that can be used for their identification. Infrared radiative transfer through thin cirrus in the window region must account for scattering processes in order to allow interpretation of the observed spectrum. In the following, we introduce approximations that can be employed to understand the transfer of infrared radiation in cloudy atmospheres.

4.6.2 Exchange of Infrared Radiation between Cloud and Surface

During the night, clouds play a critical role in modulating the surface temperature through thermal infrared radiation. To demonstrate this, we consider a configuration involving a surface with a temperature T_s. It is not a perfect blackbody but rather has an average emissivity ϵ_s. A cloud with a base temperature T_c and an average emissivity ϵ_c moves over the surface (e.g., snow). For simplicity, the effects of water vapor above and below the cloud are neglected in this discussion. Further, let the flux density emitted from the cloud and the surface be F_c and F_s, respectively, as shown in Fig. 4.13.

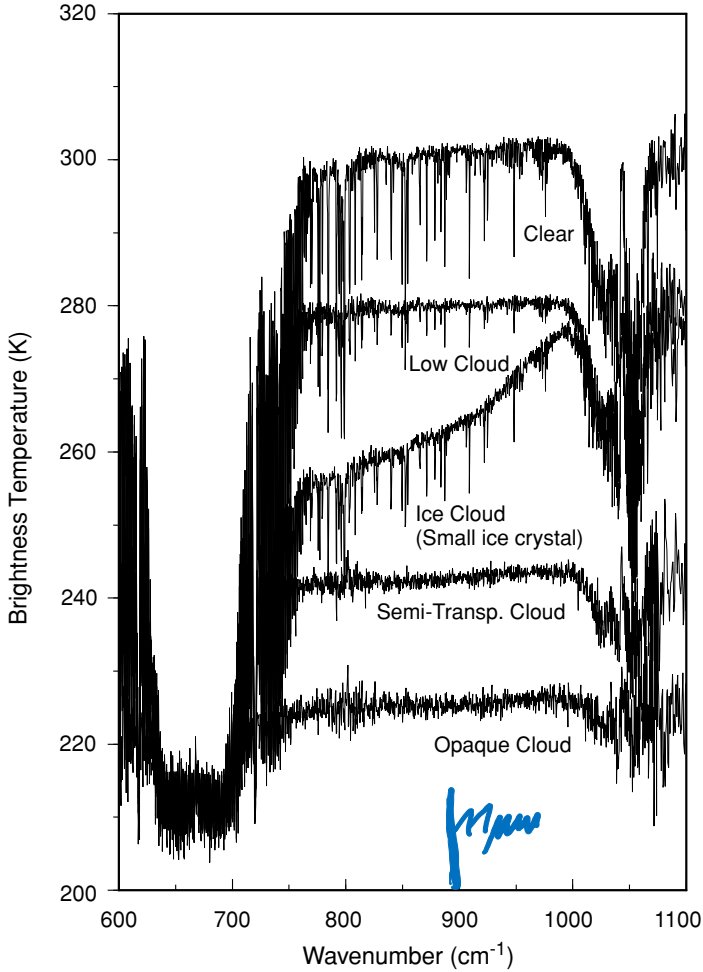

Figure 4.12 Spectra of brightness temperature observed from a high spectral resolution infrared spectrometer from the high-flying ER-2 aircraft over a domain, 37.1°–37.4° N, 95.0°–95.3° W, on April 21, 1996, indicating wavelength-dependent window brightness temperature changes according to various cloud types. The type of cloud indicated for each spectrum is identified from the Cloud Lidar System aboard the ER-2 (data taken from Smith *et al.,* 1998).

At the surface, contribution to the upward surface flux is produced by the emission from the surface plus the reflection of the flux emitted from the cloud base. Thus,

$$F_s^{\uparrow} = \epsilon_s \sigma T_s^4 + (1 - \epsilon_s) F_c^{\downarrow}. \tag{4.6.4a}$$

At the cloud base, contribution to the downward cloud flux is the sum of the emission

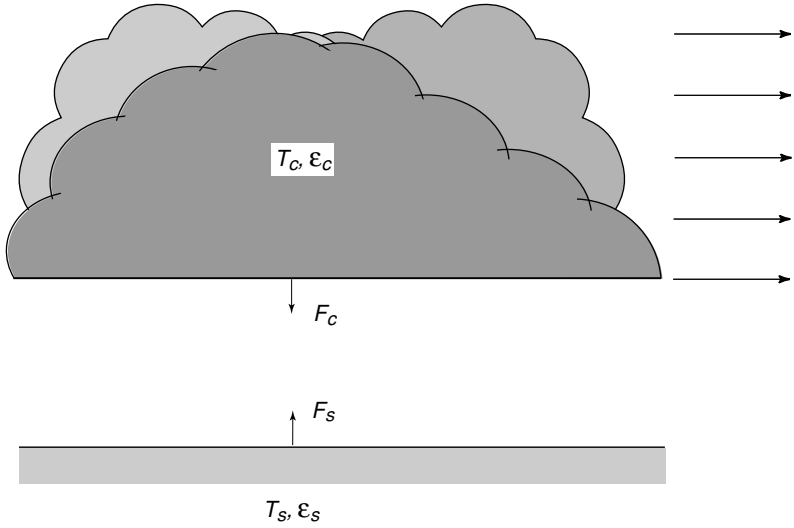

Figure 4.13 A simple configuration of a cloud moving over a surface. The surface temperature is modified by the presence of the cloud.

from the cloud and the reflection of the flux emitted from the surface. It follows that

$$F_c^{\downarrow} = \epsilon_c \sigma T_c^4 + (1 - \epsilon_c) F_s^{\uparrow}. \tag{4.6.4b}$$

In formulating the preceding equations, we have used the Stefan–Boltzmann and Kirchhoff laws. The solutions are

$$F_s^{\uparrow} = [(1 - \epsilon_s)\epsilon_c \sigma T_c^4 + \epsilon_s \sigma T_s^4]/[1 - (1 - \epsilon_s)(1 - \epsilon_c)], \tag{4.6.5a}$$

$$F_c^{\downarrow} = [(1 - \epsilon_c)\epsilon_s \sigma T_s^4 + \epsilon_c \sigma T_c^4]/[1 - (1 - \epsilon_c)(1 - \epsilon_s)]. \tag{4.6.5b}$$

Since the effects of water vapor between the cloud and the surface are neglected, the net flux in this case is then given by

$$\Delta F_n = F_s^{\uparrow} - F_c^{\downarrow} = \frac{\epsilon_c \epsilon_s}{1 - (1 - \epsilon_c)(1 - \epsilon_s)} \sigma \left(T_s^4 - T_c^4\right). \tag{4.6.6a}$$

If both the cloud and the surface are blackbodies, we can then define the cloud forcing as

$$\Delta F = \Delta F_n - \Delta F_{\text{clear}} = \sigma \left(T_s^4 - T_c^4\right) - \sigma T_s^4 = -\sigma T_c^4. \tag{4.6.6b}$$

Let the surface temperature increase due to the presence of the cloud be ΔT and assume that only infrared radiative processes take place in regulating the surface temperature. From the definition of the local heating rate, we should then have

$$\Delta T = \Delta t \left(-\frac{1}{\rho C_p} \frac{\Delta F}{\Delta z} \right). \tag{4.6.7}$$

The increase of the surface temperature ΔT is dependent on the time period Δt that the cloud remains over the snow surface and the net flux divergence $\Delta F/\Delta z$.

4.6.3 Two/Four-Stream Approximation

Combining Eqs. (4.6.1)–(4.6.3b) and using optical depth coordinates, the basic equation for the transfer of IR radiation in a scattering atmosphere may be written in the form

$$\mu \frac{dI(\tau, \mu)}{d\tau} = I(\tau, \mu) - S(\tau, \mu), \tag{4.6.8a}$$

where we have omitted the wavenumber subscript for simplicity of presentation. The source function defined in Eq. (4.6.2a) is given by

$$S(\tau, \mu) = \frac{\tilde{\omega}}{2} \int_{-1}^{1} P(\mu, \mu') I(\tau, \mu') d\mu' + (1 - \tilde{\omega}) B(\tau). \tag{4.6.8b}$$

Equation (4.6.8a) can be solved exactly by means of the discrete-ordinates or adding methods for radiative transfer presented in Chapter 6. However, we introduce here a useful and accurate approximation utilizing the two-stream approximation discussed in Section 3.4.

The phase function can be expanded in Legendre polynomials P_ℓ based on the addition theorem for spherical harmonics, as shown in Appendix E. The azimuth-independent phase function defined in Eq. (4.6.3b) is given by

$$P(\mu, \mu') = \sum_{\ell=0}^{N} \tilde{\omega}_\ell P_\ell(\mu) P_\ell(\mu'). \tag{4.6.9a}$$

In the context of the two-stream approximation, the upward and downward intensities are $I(\tau, +\mu_1) = I^{\uparrow}(\tau)$ and $I(\tau, -\mu_1) = I^{\downarrow}(\tau)$, where $\mu_1 = 1/\sqrt{3}$ based on the Gaussian quadrature. Moreover, the phase function in the limit of the two-stream approximation is given by

$$P(\mu_1, \pm \mu_1') = 1 \pm 3g\mu_1\mu_1' = 1 \pm g. \tag{4.6.9b}$$

Thus, the integration in Eq. (4.6.8b) may be replaced by

$$\int_{-1}^{1} P(\mu, \mu') I(\tau, \mu') d\mu' = (1 - g) I^{\downarrow}(\tau) + (1 + g) I^{\uparrow}(\tau). \tag{4.6.9c}$$

By expressing Eq. (4.6.8a) in terms of the upward and downward intensities, we have

$$\frac{dI^{\uparrow}(\tau)}{d\tau} = \gamma_1 I^{\uparrow}(\tau) - \gamma_2 I^{\downarrow}(\tau) - \gamma_3 B(\tau), \tag{4.6.10a}$$

$$\frac{dI^{\downarrow}(\tau)}{d\tau} = \gamma_2 I^{\uparrow}(\tau) - \gamma_1 I^{\downarrow}(\tau) + \gamma_3 B(\tau), \tag{4.6.10b}$$

where

$$\gamma_1 = [1 - \tilde{\omega}(1+g)/2]/\mu_1, \gamma_2 = \tilde{\omega}(1-g)/2\mu_1, \ \gamma_3 = (1-\tilde{\omega})/\mu_1. \quad (4.6.10c)$$

Furthermore, we may parameterize the Planck function for a predivided layer in terms of the exponential function in the form

$$B(\tau) = B_0 e^{b\tau/\tau_1}, \quad (4.6.11)$$

where $b = \ln(B_1/B_0)$ with $B_0 = B(0)$ and $B_1 = B(\tau_1)$ being the Planck functions for temperatures at the top and bottom of the layer, respectively, and τ_1 is the optical depth of this layer. The parameterization is exact at the layer's boundaries.

The solutions for the preceding two first order differential equations subject to the inhomogeneous term defined in Eq. (4.6.11) can be derived in a straightforward but involved manner. They are given by

$$I^{\uparrow}(\tau) = K\, e^{-k(\tau_1 - \tau)} + H\, a\, e^{-k\tau} + Z^{+} e^{b\tau/\tau_1}, \quad (4.6.12a)$$

$$I^{\downarrow}(\tau) = K a\, e^{-k(\tau_1 - \tau)} + H\, e^{-k\tau} + Z^{-} e^{b\tau/\tau_1}, \quad (4.6.12b)$$

where the eigenvalue of the solution and the similarity parameter are, respectively, defined by

$$k = \left(\gamma_1^2 - \gamma_2^2\right)^{1/2}, \quad a = \frac{\gamma_1 - k}{\gamma_2} = \frac{\gamma_2}{\gamma_1 + k}. \quad (4.6.12c)$$

The particular solution terms are

$$Z^{\pm} = \frac{B_0 \gamma_3 (\gamma_1 + \gamma_2 \pm b/\tau_1)}{k^2 - (b/\tau_1)^2}. \quad (4.6.12d)$$

The unknown coefficients K and H are to be determined from the radiation boundary conditions at the top and bottom of the layer. The preceding analysis constitutes the two-stream approximation for infrared radiative transfer in which we have retained the angular term $1/\mu_1$ in Eq. (4.6.10c).

Now, we return to Eqs. (4.6.8a,b) and solve the upward and downward intensities based on the integral technique illustrated in Eqs. (1.4.23) and (1.4.24). We have

$$I(0, \mu) = I(\tau_1, \mu) e^{-\tau_1/\mu} + \int_0^{\tau_1} S(\tau', \mu) e^{-\tau'/\mu} \frac{d\tau'}{\mu}, \quad (4.6.13a)$$

$$I(\tau_1, -\mu) = I(0, -\mu) e^{-\tau_1/\mu} + \int_0^{\tau_1} S(\tau', -\mu) e^{-(\tau_1 - \tau')/\mu} \frac{d\tau'}{\mu}. \quad (4.6.13b)$$

Analytic solutions are possible if specific forms for the source function terms are available. On substituting Eqs. (4.6.12a, b) into (4.6.8b) for the upward and downward intensities, respectively, and employing the two-term approximation for the integral term denoted in Eq. (4.6.9b), we obtain

$$S(\tau, \mu_1) = K\, v\, e^{-k(\tau_1 - \tau)} + H\, u\, e^{-k\tau} + Z_*^{+} e^{b\tau/\tau_1}, \quad (4.6.14a)$$

$$S(\tau, -\mu_1) = K\, u\, e^{-k(\tau_1 - \tau)} + H\, v\, e^{-k\tau} + Z_*^{-} e^{b\tau/\tau_1}, \quad (4.6.14b)$$

where

$$v = (1 - \mu_1 k),\ u = a(1 + \mu_1 k),$$
$$Z_*^{\pm} = B_0(1 - \tilde{\omega})\left[1 + \frac{\tilde{\omega}(\gamma_1 + \gamma_2 \pm gb/\tau_1)}{\mu_1(k^2 - b^2/\tau_1^2)}\right]. \tag{4.6.14c}$$

Substitution of Eqs. (4.6.14a,b) into Eqs. (4.6.13a, b) yields

$$I^{\uparrow}(0, \mu) = I(\tau_1, \mu)e^{-\tau_1/\mu} + \frac{Kv}{(1 - \mu k)}(e^{-k\tau_1} - e^{-\tau_1/\mu}) + \frac{Hu}{(1 + \mu k)}[1 - e^{-\tau_1(k+1/\mu)}] + \frac{Z_*^+}{(1 - b\mu/\tau_1)}\left(B_0 - B_1 e^{-\tau_1/\mu}\right), \tag{4.6.15a}$$

$$I^{\downarrow}(\tau_1, -\mu) = I(0, -\mu)e^{-\tau_1/\mu} + \frac{Ku}{(1 + \mu k)}[1 - e^{-\tau_1(k+1/\mu)}] + \frac{Hv}{(1 - \mu k)}(e^{-k\tau_1} - e^{-\tau_1/\mu}) + \frac{Z_*^-}{(1 + b\mu/\tau_1)}\left(B_1 - B_0 e^{-\tau_1/\mu}\right). \tag{4.6.15b}$$

By employing the two-stream approximation for the source function, we have demonstrated that the upward and downward intensities can be solved analytically. Moreover, for flux calculations, we may select two-stream in the upward direction and two-stream in the downward direction based on the double Gaussian quadrature such that the discrete directions $\mu = 0.2113248$ and 0.7886752, and the weight $a = 0.5$ for both directions. This constitutes the four-stream approximation in which the upward and downward fluxes are given by

$$F^{\uparrow}(\tau) = \int_0^1 I(\tau, \mu)\mu d\mu \cong \sum_{i=1}^{2} I^{\uparrow}(\tau, \mu_i)\mu_i a_i, \tag{4.6.16a}$$

$$F^{\downarrow}(\tau) = \int_0^{-1} I(\tau, \mu)\mu d\mu \cong \sum_{i=1}^{2} I^{\downarrow}(\tau, -\mu_i)\mu_i a_i. \tag{4.6.16b}$$

The methodology that combines the two-stream technique for the source function and the four-stream method for flux calculations is referred to as the *two/four-stream approximation* for radiative transfer. For infrared flux calculations, it suffices to use the diffusivity factor $1/\bar{\mu}$ of 1.66 to represent the inverse of the mean emergent angle of μ_1 that appears in the preceding equations. The use of 2 for $1/\bar{\mu}$ has also been suggested, which is more consistent with the four-stream approximation such that $\sum \mu_i/2 = \bar{\mu}$. However, in the context of the two/four-stream approximation, the use of 1.66 and 2 for $1/\bar{\mu}$ for flux calculations is similar. Further, to improve the representation of the phase function for the scattering of cloud particles based on a single parameter, namely the asymmetry factor, we may apply the delta-function adjustment based on the similarity principle for radiative transfer, introduced in Section 6.5.3, to adjust the optical depth, single-scattering albedo, and asymmetry factor. The delta two/four-stream approach has been shown to be an accurate and efficient means for the calculation of infrared

fluxes in cloudy conditions (Fu *et al.,* 1997; Toon *et al.,* 1989). Its accuracy, however, is less satisfactory for the calculation of solar flux transfer because of the strong anisotropic nature of the scattering phase function for cloud particles (see Section 6.5.4 for further discussion). In the following, we present some pertinent results for infrared cooling rates in typical clear and cloudy conditions and discuss the accuracy of the delta two/four-stream approximation.

4.7 Atmospheric Infrared Cooling Rates

Because the atmosphere loses radiative energy to space through thermal infrared emission, it is normally cooled by such processes. Thus, we speak of the infrared cooling rate (or negative heating rate) in the discussion of radiative transfer. Analogous to the solar heating rate defined in Eq. (3.5.3), we may define the infrared cooling rate in the form

$$\left(\frac{\partial T}{\partial t}\right)_{ir} = -\frac{1}{\rho C_p}\frac{dF(z)}{dz}, \tag{4.7.1}$$

where the net infrared flux at a given height is defined by

$$F(z) = F^{\uparrow}(z) - F^{\downarrow}(z), \tag{4.7.2}$$

and the upward and downward infrared fluxes covering the entire thermal infrared spectrum have been defined in Eq. (4.2.11). In what follows, we present a number of representative infrared cooling rate profiles computed from the line-by-line (LBL) method and the correlated *k*-distribution (CKD) method.

Figures 4.14a, 4.14c, and 4.14e show the heating rate profiles computed using LBL integration for H_2O (0–2200 cm^{-1}), CO_2 (540–800 cm^{-1}), and O_3 (980–1100 cm^{-1}), respectively. Cooling rates produced by water vapor lines are seen in the troposphere and the middle atmosphere. A significant variability is shown for the four atmospheric humidity and temperature profiles used in the calculations. The maximum and minimum patterns located at about 50 km are related to the temperature inversion (see Fig. 3.1). In the lower atmosphere, cooling rates range from 1 to 2 K day^{-1}, and are primarily produced by the rotational band of water vapor. Carbon dioxide generates significant cooling rates in the middle atmosphere where the temperature profile is an important factor in determining flux exchanges. At about 50 km, a cooling rate of about 10 K day^{-1} is seen. The ozone cooling rate profile is governed by the ozone concentration, which has a maximum located at about 20–25 km, resulting in a small amount of positive heating.

Figures 4.14b, 4.14d, and 4.14f show the corresponding error profiles for the results computed using CKD. From the LBL results, it is clear that infrared cooling rates in

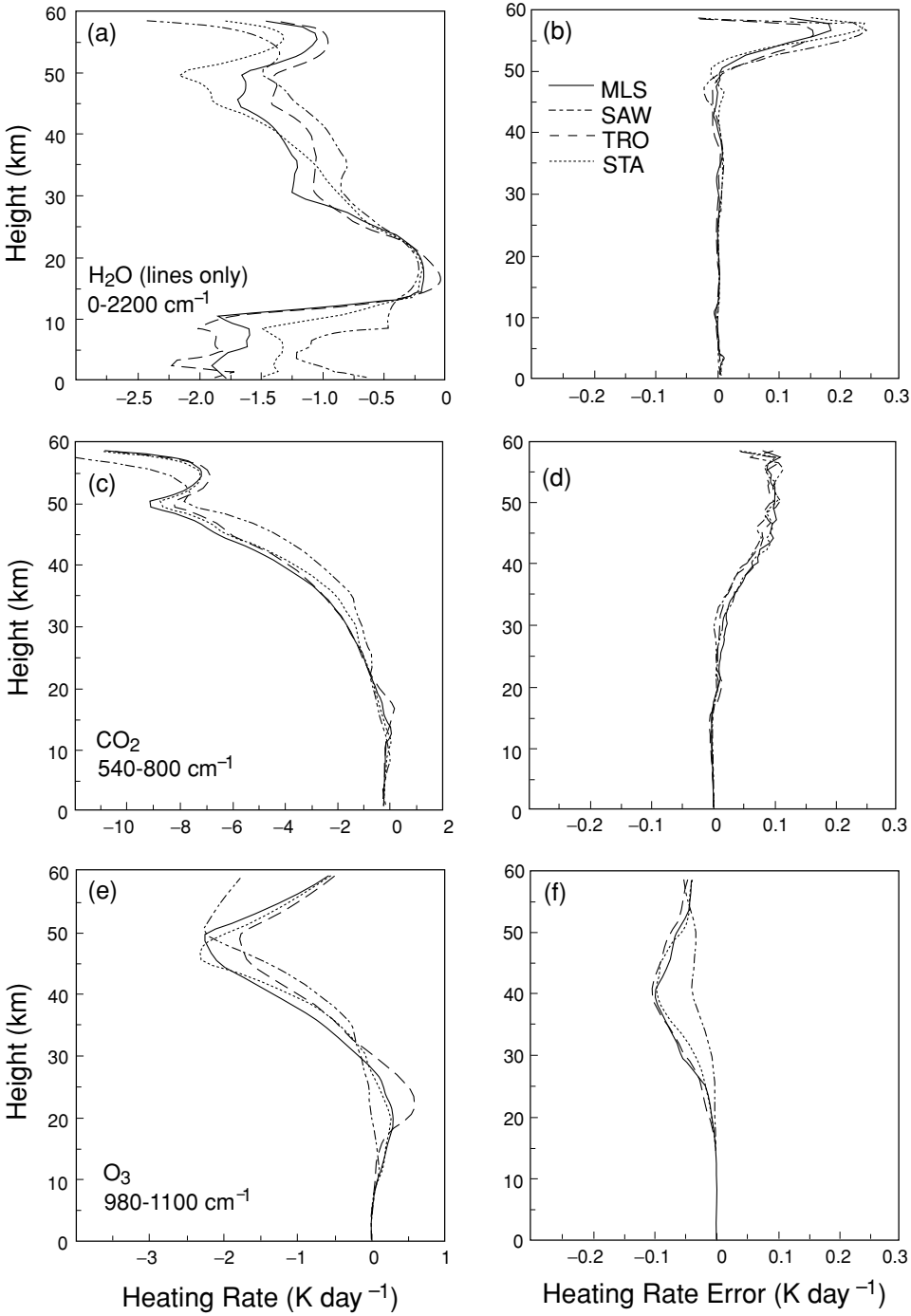

Figure 4.14 Heating rate profiles computed from LBL and the error profiles produced by CKD for the H_2O (a and b), CO_2 (c and d), and O_3 (e and f) bands in the infrared spectrum for the midlatitude summer (MLS), subarctic winter (SAW), tropical (TRO), and U.S. Standard (STA) atmospheres (data taken from Fu and Liou, 1992).

the troposphere are primarily produced by H_2O. In the stratosphere, H_2O, CO_2, and O_3 contribute ~15%, 70%, and 15% of the total cooling in the vicinity of the 50–km region, respectively. For H_2O, errors in the heating rates calculated by CKD are less than ~0.01 K day^{-1} in the troposphere and stratosphere, and less than ~0.24 K day^{-1} above the stratopause, as shown in Fig. 4.14. The relatively large errors above the stratopause may be explained by the fact that at lower pressure regions the atmosphere is thinner and more transparent and as a result, distant layers would affect cooling more significantly. As shown in Fig. 4.14, errors in the CO_2 cooling rates produced by CKD in the troposphere and lower stratosphere are ~0.01 K day^{-1}, while the errors above 30 km are less than ~0.1 K day^{-1}. For O_3, the heating rates computed from CKD are also in excellent agreement with those from LBL. The differences are less than ~0.1 K day^{-1}. CKD yields the most accurate results in the subarctic winter atmosphere due to the O_3 9.6-μm band. This can be explained by the larger amount of ozone in the subarctic winter atmosphere, which leads to stronger absorption and a more opaque atmosphere.

In Fig. 4.15, we display infrared cooling rate profiles for clear sky employing the midlatitude summer atmosphere, representing a relatively moist condition, and the subarctic winter atmosphere, representing a dry condition. The vertical resolution used in the calculation was 0.25 km. Calculations were made from a line-by-line equivalent multiple scattering program. Substantial differences are shown for these two profiles. For the former, cooling rates are on the order of 2 K day^{-1}, with the largest cooling of about 3 K day^{-1} near the surface produced by the rotational band of water vapor and continuous absorption principally in the 10 μm window. For the latter, cooling rates are only on the order of about 1 K day^{-1}. When clouds are present, significant cooling/heating takes place in the cloud region. In the low cloud condition, cloud top cooling reaches 35 K day^{-1}, generated from the flux exchange between the air above the cloud and the optically black cloud. Because the low cloud base (1 km) is close to the surface, cloud base heating is extremely small. In the middle cloud condition, however, a large cooling rate of about 60 K day^{-1} occurs at the cloud top coupled with a heating rate of about 16 K day^{-1}, resulting from the trapping of longwave flux emitted from the warmer surface and lower atmospheres. Because of a lower ice-water content in the case of high clouds, smaller cloud top cooling and cloud bottom warming, each with a value of about 4 K day^{-1}, are shown. These results clearly reveal the importance of clouds in the generation of cooling/heating rates that are directly related to their dynamic and physical processes in the atmosphere.

Finally, we present an example of infrared flux measurements from aircraft along with their theoretical interpretation. Measurement of the atmospheric heating/cooling rate from an aircraft platform is a difficult task. It requires calibrated broadband flux radiometers to perform upward and downward flux measurements during the course of aircraft operation. It is particularly difficult for the measurement of solar flux owing to the geometry of the sun with respect to the radiometer on the aircraft. Moreover, the heating/cooling rate is a result of net flux divergence, which is the difference of two close values. Because of the inherent uncertainty in radiometric instrumentation, heating/cooling rates derived from flux measurements usually contain substantial

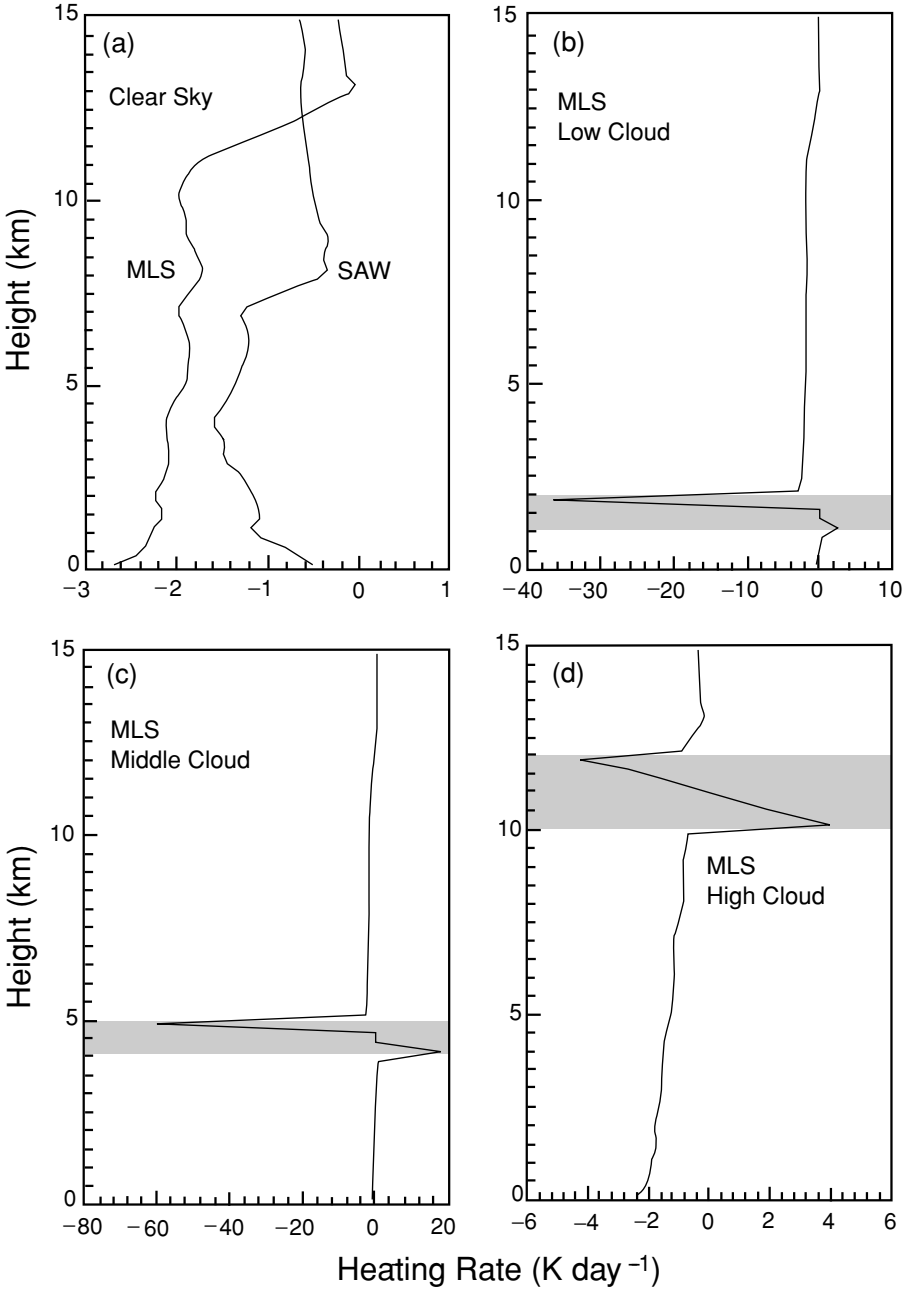

Figure 4.15 (a) Total cooling rates for the midlatitude summer (MLS) and subarctic winter (SAW) atmospheres in clear sky. (b), (c), and (d) display cooling rate profiles for the MLS atmosphere containing low, middle, and high clouds, respectively. The liquid (ice) water content and mean effective radius (size) for these clouds used in the calculations are (0.22 g m^{-3} and 5.89 μm), (0.28 g m^{-3} and 6.2 μm), and (0.0048 g m^{-3} and 41.5 μm), respectively. The locations of these clouds are shaded (data taken from Fu *et al.,* 1997).

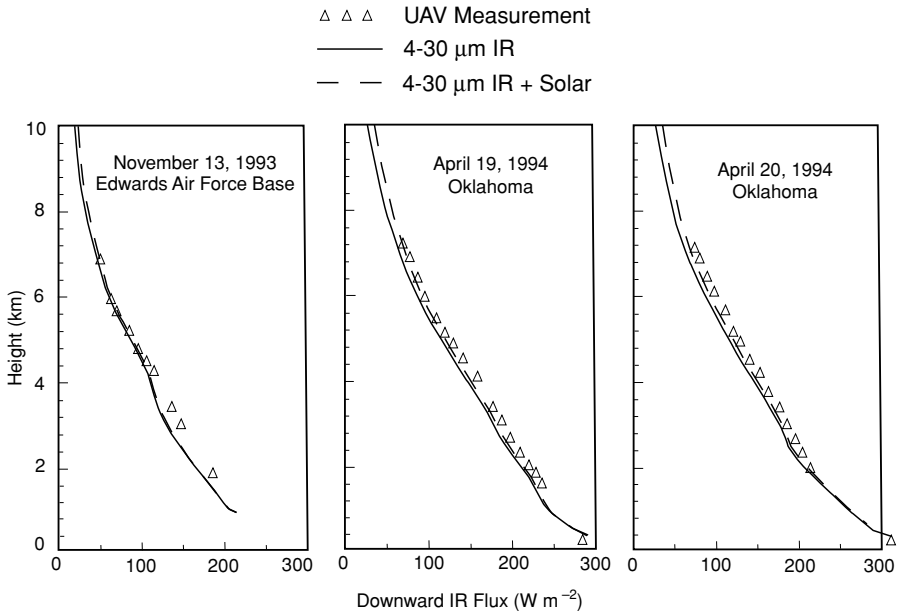

Figure 4.16 Downward infrared fluxes obtained from the measurements of unmanned aerospace vehicle (UAV) and from theoretical results for a spectral region covering 4–30 μm with and without including the solar radiation contribution (based on an interim report K. N. Liou submitted to P. Crowley and J. Vitko of the Department of Energy, June 1995).

uncertainty. In the following, we present downward infrared fluxes derived from radiometers on board an unmanned aerospace vehicle that was flown on a number of days and locations as indicated in Fig. 4.16. Downward infrared fluxes increase with decreasing altitude, signifying the emission contribution from the atmosphere. Theoretical results are computed by using the correlated k-distribution method along with observed temperature and moisture profiles collected from nearby soundings. There is a general agreement between the computed and measured downward infrared flux profiles, particularly when the contribution of solar flux is accounted for in the theoretical calculation. In Table 2.3, we show that there are about 11 W m^{-2} of solar energy contained in the wavelengths greater than 4 μm. This energy has been ignored in thermal infrared radiative transfer calculations when comparisons with radiometric measurements are made. Deviation in the lower atmosphere in the case of Edwards Air Force Base is due to uncertainty of the moisture profile data available from distant sounding.

In summary, to cross check theoretical heating/cooling calculations from the line-by-line or the correlated k-distribution models, we must have reliable and verifiable flux measurements from aircraft, an area that requires further advances in spaceborne radiometric technology.

Exercises

4.1 Table 4.1 lists the line-by-line data from HITRAN 96 (Rothman *et al.,* 1998) for a 10 cm^{-1} interval in the 1.38 μm H_2O band. (a) Using the Lorentz line shape, plot the absorption coefficient k_ν as a function of wavenumber in this interval. (b) Divide k_ν in the logarithmic scale into 50 equal intervals and compute the total cumulative number $n(0, k)$ of k_ν in progressive intervals. (c) The cumulative probability function is defined by $g(k) = n(0, k)/N$, where N is the total number such that $g(0) = 0$ and $g(50\Delta \log k) = 1$. Plot $k(g)$ in the g-domain.

Table 4.1

HITRAN 96 Line Data for a 10 cm^{-1} Interval in the 1.38 μm Band for $p = 1013$ mb and $T = 296$ K

ν_0 (cm^{-1})	S [cm^{-1}/(atm cm)]	α(cm^{-1})
7280.31512	4.194E-03	0.0704
7280.47400	8.872E-04	0.0846
7281.08200	3.764E-02	0.0994
7281.72912	4.033E-03	0.0602
7282.70531	5.673E-04	0.0752
7283.01859	1.132E-02	0.0680
7283.73107	1.710E-02	0.0710
7284.71668	2.401E-03	0.0702
7285.04497	4.275E-04	0.0866
7286.05083	4.732E-03	0.0683
7287.00300	6.990E-03	0.0886
7287.28900	2.285E-02	0.1020
7287.50218	2.877E-04	0.0685
7288.09091	6.882E-02	0.1002
7290.10832	3.226E-02	0.0872

Table 4.2

The Quadrature Points and Weights for Integrals in the g-Domain (0,1)

Quadrature points	Quadrature weights
3.20770E-02	8.13791E-02
1.60926E-01	1.71362E-01
3.61656E-01	2.22259E-01
5.88344E-01	2.22259E-01
7.89074E-01	1.71362E-01
9.17923E-01	8.13791E-02
9.53472E-01	8.69637E-03
9.66501E-01	1.63036E-02
9.83500E-01	1.63036E-02
9.96528E-01	8.69637E-03

(d) Compute the spectral transmittance from the line-by-line approach employing an interval of 0.01 cm^{-1} and from the k-distribution method using quadrature points and weights listed in Table 4.2. Use the path length u from 10^{-5} to 10 (g cm^{-2}). Compare the two results. Note that 1 (g cm^{-2}) is $2.24 \times 10^4/M$ (atm cm), where M is the molecular weight of the gas.

4.2 (a) Show that the equivalent width of a single Lorentz line is given by $W = 2\pi\alpha L(x)$, where $L(x)$ is the Ladenberg and Reiche function, and $x = su/2\pi\alpha$. (b) From the property of the Bessel function, show that the equivalent width is proportional to u and $\sqrt{u}$, respectively, in the limits of weak- and strong-line approximations.

4.3 Given the absorption coefficient expressed in the Elsasser regular band model [Eq. (4.4.10)], derive the probability function $f(k)$ for this case.

4.4 (a) From the Malkmus model defined in Eq. (4.4.34b), show that the probability distribution function can be derived from the inverse Laplace transform given by

$$f(k) = \frac{1}{2\sqrt{\pi}} c_{\bar{\nu}} d_{\bar{\nu}}^{1/2} k^{-3/2} \exp\left(c_{\bar{\nu}} - k/d_{\bar{\nu}} - c_{\bar{\nu}}^2 d_{\bar{\nu}}/4k\right).$$

(b) Show that the cumulative probability function is given by

$$g(k) = \frac{1}{2} e^{2c_{\bar{\nu}}} \text{erfc}\left[\left(\frac{c_{\bar{\nu}}}{2}\right)^{1/2}\left(\frac{1}{y} + y\right)\right] + \frac{1}{2}\text{erfc}\left[\left(\frac{c_{\bar{\nu}}}{2}\right)^{1/2}\left(\frac{1}{y} - y\right)\right],$$

where $y = [2k/(c_{\bar{\nu}} d_{\bar{\nu}})]^{1/2}$. The notation erfc is the complementary error function given by $\text{erfc}(x) = 1 - \text{erf}(x)$, and the error function is defined by

$$\text{erf}(x) = \frac{2}{\sqrt{\pi}} \int_0^x e^{-x^2}\, dx.$$

(c) From (b), show that $dg(k)/dk = f(k)$.
(d) Derive the inverse Laplace transform of the spectral transmittance under the limits of weak- and strong-line approximations defined in Eq. (4.4.33).

4.5 Consider a simplified Voigt profile by combining a rectangular Doppler core (with a value of C) with Lorentzian wings as follows:

$$f_\upsilon(\nu) = \begin{cases} C, & |\nu| \le \nu_0, \\ \alpha/\pi\nu^2, & |\nu| > \nu_0. \end{cases}$$

Derive the equivalent width for Goody's random model.

4.6 The half-width of a Lorentz line is proportional to pressure and can be expressed by $\alpha \cong \alpha_r(p/p_r)$, where α_r is the half-width at the reference pressure p_r. Show

that the optical depth may be expressed by

$$T_\nu = e^{-\tau} = \left[\left(\nu^2 + \alpha_1^2\right)/\left(\nu^2 + \alpha_2^2\right)\right]^\lambda,$$

where α_1 and α_2 are two integration limits and $\lambda = Sp_r q/(2\pi g\alpha_r)$, with q the mixing ratio and g the gravitational acceleration.

4.7 (a) With the strong-line approximation limit $\bar{S}u/\alpha \gg 1$, show that

$$T_{\bar{\nu}}(u) = \exp(-\sqrt{\pi \bar{S}\alpha u}/\delta).$$

This is referred to as the *square root approximation for the random model*. (b) Based on this approximation, show that the precipitable water in cloudy atmospheres may be determined from

$$PW = (c/m)\left[\ln(F_{\bar{\nu}}/F_{0,\bar{\nu}})\right]^2,$$

where c is a constant related to the band and known atmospheric parameters, m denotes the air mass, which is related to pressure, and $F_{\bar{\nu}}$ and $F_{0,\bar{\nu}}$ represent the observed solar flux in the 0.94 μm band at the ground and at the top of the atmosphere, respectively. This is the principle of the sunphotometer for the measurement of precipitable water.

4.8 Using the probability function

$$P(S) = \frac{C}{S} e^{-s/\bar{s}},$$

where C is a normalization factor, show that the average equivalent width is given by

$$\bar{W} = c_{\bar{\nu}}\left[(1 + d_{\bar{\nu}}u)^{1/2} - 1\right],$$

where $c_{\bar{\nu}} = \pi\alpha/2\delta$ and $d_{\bar{\nu}} = 4\bar{S}/\pi\alpha$. In the derivation, use the following integration formulas:

$$\int_0^\infty e^{-ax} \frac{1 - e^{-x}}{x} dx = \ln(1 + 1/a),$$

$$\int \ln(x^2 + b)\, dx = x \ln(x^2 + b) - 2x + 2\sqrt{b} \tan^{-1}(x/\sqrt{b}).$$

Based on the procedure outlined in Section 4.4.3, determine the coefficients $c_{\bar{\nu}}$ and $d_{\bar{\nu}}$ from the line-by-line data.

4.9 From the definition of the Voigt profile, derive Eq. (4.4.45). In the derivation, set $\cos \nu t = \cos\left[(\nu - \nu') + \nu'\right]t$.

4.10 The spectral transmittance defined in Eq. (4.3.20a) can be written in the form

$$T_{\bar{\nu}}(q, q_c) = \int_0^\infty f_2^*(k'')dk'' \int_{k''}^\infty e^{-ku_1} f_1(k - k'')\, dk.$$

By changing the order of integrals such that the resulting areas of the integrations remain the same, derive Eq. (4.3.20c) via the convolution theorem of the Laplace transform given in Eq. (4.3.20b).

4.11 Derive Eqs. (4.6.12a,b) from Eqs. (4.6.10a,b). This is the two-stream approximation for thermal infrared radiation transfer.

Suggested Reading

Elsasser, W. M., and Culbertson, M. F (1960). Atmospheric radiation tables. *Meteorol. Monog*. **4** (23), 1–43. This monograph provides essential information on the transfer of infrared radiation and broadband emissivity values.

Goody, R. M., and Yung, Y. L. (1989). *Atmospheric Radiation. Theoretical Basis,* 2nd ed. Oxford University Press, New York. Chapters 3–5 contain authoritative and fundamental discussions of the theory of gaseous absorption and band models.

Kondratyev, K. Ya. (1969). *Radiation in the Atmosphere* (International Geophysics Series, Vol. 12). Academic Press, New York. Gaseous absorption and infrared radiative transfer are discussed in Chapters 3 and 9.

Liou, K. N. (1992). *Radiation and Cloud Processes in the Atmosphere. Theory, Observation, and Modeling*. Oxford University Press, New York. Chapter 2 provides a more detailed presentation of the band models and emissivity parameterizations.